Annu. Rev. Mater. Res. 2007.37:93-126. Downloaded from arjournals.annualreviews.org
by University of Virginia Libraries on 02/20/08. For personal use only.

Microscale Characterization of Mechanical Properties

K.J. Hemker and W.N. Sharpe, Jr.

Department of Mechanical Engineering, Johns Hopkins University, Baltimore, Maryland 21218; email: hemker@jhu.edu, sharpe@jhu.edu

Annu. Rev. Mater. Res. 2007. 37:93–126

First published online as a Review in Advance on February 20, 2007

The *Annual Review of Materials Research* is online at http://matsci.annualreviews.org

This article's doi:
10.1146/annurev.matsci.36.062705.134551

Copyright © 2007 by Annual Reviews.
All rights reserved

1531-7331/07/0804-0093$20.00

Key Words

size effects, microtensile testing, Young's modulus, strength, microelectromechanical systems (MEMS), experimental techniques, high temperature

Abstract

Lilliputian techniques for measuring the mechanical response of microscale specimens are being developed to characterize the performance and reliability of microelectromechanical systems (MEMS) and other small-scale entities. The challenges associated with the preparation, handling, and testing of small volumes of material have spawned a variety of techniques; this review focuses on uniaxial testing. Results from these experiments provide valuable insight into size-scale effects on the elastic, brittle, and ductile behavior of micron-sized structures. Fundamental elastic interactions show no size effect; in-plane moduli can be predicted from anisotropic elastic constants if crystallographic texture is properly considered. Intrinsic fracture toughness is also size independent, although the fracture strength of brittle MEMS materials is extremely dependent on flaw size and distribution. By contrast, size effects on the strength of ductile materials suggest that the operation of intrinsic dislocation processes in greatly reduced or confined volumes alters their generation, multiplication, interaction, and motion.

INTRODUCTION

MEMS: microelectromechanical systems

Microscale: length scale in the range of 1–1000 microns

Efforts to characterize the small-scale and scale-specific mechanical properties of materials are driven by (*a*) the need to reliably predict the performance of micro-electromechancial systems (MEMS) and other microscale devices and (*b*) a desire to develop detailed and accurate hierarchical models of the mechanical behavior of complex, multicomponent structural materials. In both cases, the development of microscale experiments is motivated by the need to measure the mechanical behavior of small volumes of material and by a desire to determine how, if at all, the mechanical properties of a material change when external dimensions and internal microstructural features are greatly reduced.

Significant challenges related to the preparation and handling of microspecimens, the application of controlled amounts of force to deform these microspecimens, and the accurate measurement of stress and strain in these specimens all must be overcome to obtain a reliable measure of the mechanical properties of small volumes of materials. These challenges not withstanding, reliable microscale testing techniques have begun to emerge and are being used to determine the mechanical properties of a wide range of materials and to investigate the importance of size on the mechanical behavior. Here we provide an introduction to various testing techniques that have been developed to measure the mechanical response of small specimens. This review focuses on uniaxial microscale experiments; it outlines procedures that have been developed to conduct these experiments, presents various examples to illustrate recent successes in this area, and contains an initial discussion of size-scale effects on mechanical properties.

EXPERIMENTAL TECHNIQUES FOR MICROSCALE TESTING

Efforts to characterize the mechanical response of small volumes of materials have led to the development and use of a variety of test methodologies. These methodologies are reviewed briefly here, but the reader is referred to the excellent reviews that exist on many of these topics for more in-depth discussion (see, for example, References 1–4). This review emphasizes the use of uniaxial microspecimens that experience uniform stresses and strains in the gauge when loaded in either tension or compression. These experiments closely mimic the ASTM tests (5) that are used in the macro world and are most straightforward to interpret.

A Survey of Microscale Test Methodologies

Vickers and other microhardness measurements are confined to small volumes and do provide an indication, if not a direct measure, of mechanical properties. The hardness of a material, however, is affected by its stiffness, strength, and propensity to strain harden. Complications associated with the nonuniform distribution of stresses under the tip of the indenter make it hard to separate the influence of these individual properties. The introduction of instrumented indentation, most specifically

Annu. Rev. Mater. Res. 2007.37:93-126. Downloaded from arjournals.annualreviews.org
by University of Virginia Libraries on 02/20/08. For personal use only.

nanoindentation, has made it possible to interrogate extremely small volumes of material. Use of this technique coupled with careful attention to the loading and unloading response of a material make it possible to measure both the hardness and elastic modulus of a material (see, for example, References 6–12). Although many models have been proposed, strength and strain hardening cannot be directly measured with indentation techniques. However, efforts at modeling indentation size effects in terms of mechanism-based strain gradient plasticity (13–15) may provide an important pathway for using nanoindentation measurements to provide material-specific parameters for constitutive modeling.

Nanoindentation experiments have found broad application in the interrogation of thin films on hard substrates, as are often found in microelectronic devices. The microelectronics industry has also made extensive use of thermal cycling experiments of thin metallic films on Si substrates. The coefficient of thermal expansion (CTE) mismatch between the film and substrate, differences in elastic properties, and the temperature dependence of yield and creep strengths all contribute to the thermal cyclic response of these structures. The response to thermal cycling of Al thin films is substantially different than is predicted by consideration of the pertinent deformation mechanisms (yielding, creep, etc.) (16). The confinement associated with the thin film geometry appears to play an important role and has received much attention in recent years; Freund & Suresh (17) review this subject.

Investigators have also studied the mechanical response of polycrystalline thin films deposited on compliant substrates (18–21). An example of these types of experiments is given by Hommel & Kraft (19), who tested 0.4–3.2-μm-thick by 6-mm-wide Cu films deposited on a 125-μm-thick polyimide film. The polyimide is significantly more compliant than the metal and imposes a strain on the film when loaded in uniaxial tension. In situ X-ray diffraction experiments allow for the measurement of elastic stresses, crystallographic texture, and evolution of dislocation densities in the Cu film, whereas overall elongation is determined with a laser extensometer. Specimens are typically elongated in increments of 10 μm and then held for some time while the X-ray data are collected. The constraint of the polyimide on the metal film and the relaxations that occur during these holds must be accounted for and can lead to responses that are different than what occurs in freestanding thin films. Nevertheless, the importance of these types of experiments is expected to rise as flexible electronics become commercially viable.

Vlassak and colleagues have promoted the use of thin film bulge testing to measure the elastic and plastic response of substrate-free thin films. They originally showed how the elastic response (Young's modulus and Poisson's ratio) could be obtained by comparing the response of square and rectangular films (22). More recently they used the plane-strain conditions in the middle of a rectangular-shaped membrane to determine the flow characteristics of bare and passivated Cu thin films (23–25). Use of this technique is dependent on relatively complex models of the boundary conditions and requires very accurate measures of geometry and displacement. Jayaraman et al. (26) used bulge testing to measure the elastic modulus and Poisson's ratio of polysilicon, and Edwards and colleagues (27) have shown that bulge tests and microtensile tests produce the same modulus values for silicon nitride films.

Annu. Rev. Mater. Res. 2007.37:93-126. Downloaded from arjournals.annualreviews.org
by University of Virginia Libraries on 02/20/08. For personal use only.

Annu. Rev. Mater. Res. 2007.37:93-126. Downloaded from arjournals.annualreviews.org
by University of Virginia Libraries on 02/20/08. For personal use only.

FIB: focused ion beam

Difficulties associated with the handling of small specimens and a desire for on-chip testing have led investigators to consider other inverse methods to determine mechanical properties. In addition to the bulge test, thin film cantilevers have been tested in resonance and by monotonic loading (pressing on the end of the beam with the tip of a nanoindenter) (see, for example, References 28–30). As compared with tensile specimens, for which large forces are required to produce small axial elongations, cantilever beams produce much larger deflections at lower loads. Bending a cantilever beyond its elastic response will result in localized plastic deformation or fracture and can be used to measure the material's strength. However, this measurement may depend on the volume of material that is being interrogated, which is inherently small in bending experiments. Techniques for machining a crack at the base of a beam with focused ion beam (FIB) machining are being developed to measure more accurately the fracture toughness of thin film materials. As with all indirect techniques, the accuracy of these measurements is highly dependent on the boundary conditions and the geometry of the cantilever, and this uncertainty appears to be the greatest challenge to the use of this technique.

MEMS manufacturers have pushed for an electronic measure of material properties that can be used for quality control; the M-test (31) is an example of such a test. It involves a thin strip of material that is attached at both ends and suspended above the substrate in the middle. The strip snaps down onto the substrate when a sufficiently high voltage is applied, and determination of the snap-down voltage can serve as an indirect measure of the mechanical properties of the strip. Like indentation, the stress state in this structure is nonuniform and depends on other factors, namely differences between nominal and true microscopic dimensions and difficulties associated with modeling the boundary conditions of an experimental device. This is a recurring theme for indirect techniques. By comparison, tensile and compression tests have advantages in simplicity and the generation of a uniform stress state, which is why they are the standard method for determining mechanical properties of macroscopic structural materials and are the focus of the remainder of this paper.

Experimental Challenges in Microscale Testing

Tensile testing at the microscale is quite different from the familiar ASTM standard tests for structural materials. One cannot simply cut a specimen from a billet or component, place it in a commercial test machine, and push the computer ENTER key. In the macro world, force is easily measured with load cells, strain can be obtained with foil gauges or extensometers, and furnaces that fit the test machine are readily available if high-temperature properties are needed. Challenges of testing at the microscale include microspecimen preparation and handling, the application of small forces, stress and strain measurement, and elevated temperature testing. Examples of how these issues can be addressed are described below.

Microspecimen Preparation and Handling

The preparation of MEMS test specimens naturally follows the processes used in manufacturing MEMS devices, which are similar to those found in the microelectronics

Annu. Rev. Mater. Res. 2007.37:93-126. Downloaded from arjournals.annualreviews.org
by University of Virginia Libraries on 02/20/08. For personal use only.

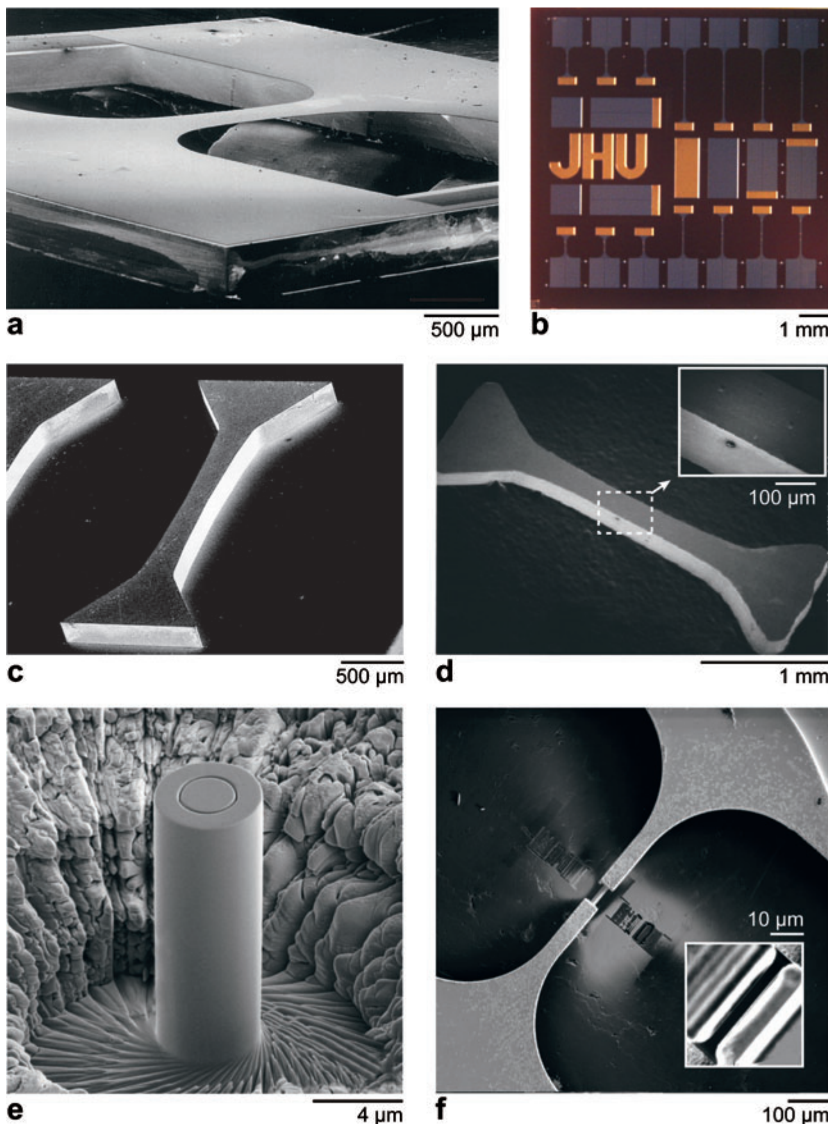

Figure 1

(*a*) A polysilicon framed microtensile specimen with a 3-μm-by-500-μm gauge (32). (*b*) Fourteen surface machined 3-μm-by-50-μm polysilicon microtensile specimens of varying length (34). (*c*) A LIGA Ni bowtie-shaped microtensile specimen with a 200-μm-by-200-μm gauge. (*d*) A bowtie-shaped specimen of nanocrystalline Ni with a 200-μm-by-200-μm gauge. (*e*) A 5-μm-diameter focused ion beam (FIB) machined single-crystalline Ni microcompression specimen (photo courtesy of M. Uchic). (*f*) A framed microtensile specimen of single-crystalline Au with a 5-μm-by-5-μm FIB machined gauge section in the center of the specimen (photo courtesy of C. Eberl).

industry. Such processes are usually a combination of both additive and subtractive processes, i.e., the material is deposited onto a substrate, the specimen is patterned by photolithographic processes, and the unwanted material is etched away. Sharpe et al. (32) describe the processes involved in detail. An example is the thin, but wide and long, polysilicon tensile specimen shown in **Figure 1*a***. The framed specimen is easily handled, the gauge section in the middle enables measurement of both Young's modulus and Poisson's ratio, the large ends are fastened into a test machine, and the two supporting strips can be cut to leave a freestanding specimen.

Similarly, framed nanocrystalline Al microtensile specimens with thicknesses of 100–300 nm have been fabricated with the following process flow (33). A 4-μm-thick thermal silicon dioxide layer is grown on a Si wafer and used as a mask for backside KOH etching that was stopped with 50 μm of Si remaining to provide support for front-side patterning and film deposition. A liftoff technique is used to pattern the microsample geometry, and the desired nanocrystalline metallic film is sputtered on top of the photoresist, which is dissolved away in acetone. Finally, a pulsed dry gas etchant of XeF_2 is used to remove the supporting Si layer and reveal the freestanding thin film. Lines patterned around the outside of the specimen simplify separation of the dies along preferred crystallographic orientations.

Nanocrystalline: polycrystalline materials with grain sizes in the range of 1–100 nm

Microtensile specimens: mechanical test specimens that possess a well-defined gauge section with cross-sectional dimensions of one to several hundred microns and that are loaded in uniaxial tension

ISDG: interferometric strain displacement gauge

DRIE: deep reactive ion etching

EDM: electrode discharge machining

Figure 1*b* shows a narrower polysilicon specimen sample (34). Such a sample does not allow lateral strain measurement by the interferometric strain/displacement gauge (ISDG) but is considerably cheaper because more specimens can be produced on a single die, which is also easily handled. The die is mounted in the fixed grip of the test machine. One end of the specimen remains attached to the die, and the other end is attached to the movable grip by gluing a 140-micron silicon carbide fiber to it. The specimen is fabricated by the same methods as the wider ones, with one important exception: It is released by front-side etching, so holes must be included in the grip to allow the etchant to reach the underlying substrate.

Additive and subtractive processes are also used to prepare thicker specimens of MEMS materials. Pure Ni and some Ni alloys can be electroplated into molds to make microtensile specimens that are robust enough to be handled with tweezers and have wedge-shaped ends that fit into the matching grips of a small test machine. **Figure 1*c*** shows a Ni bowtie-shaped microtensile specimen that is 3 mm long and has a gauge cross section of 200 μm by 200 μm (35). This batch of specimens was electroplated into SU8 molds on a Si wafer that were produced by exposure to X rays from a synchrotron. This process, referred to as LIGA, can be used to produce microstructures with in-plane tolerances of less than a micron and thicknesses of hundreds of microns (36).

Deep reactive ion etching (DRIE) is a subtractive process, provides submicron in-plane resolution, and can also be used to fabricate MEMS structures or microtensile specimens that are hundreds of microns thick (37). DRIE is most commonly associated with the micromachining of single-crystalline Si but can also be used to shape other materials. For example, thin (∼100-μm-thick) silicon carbide wafers have been patterned and etched to make microtensile specimens for fracture strength measurements at room temperature and 1000°C (38).

Microtensile specimens can also be extracted from a specific region or phase in a larger billet or component but must be prepared by subtractive methods that do not change the properties of the material to be tested. Traditional machining techniques produce a damaged layer on the finished surface that is comparable to the volume of material to be tested. Experience has shown that techniques used to prepare TEM thin foils translate well to the preparation of microtensile specimens. Diamond saws, electrode discharge machining (EDM), and tripod polishing have been used to prepare freestanding microtensile specimens from a wide range of materials, including but not limited to base metal, recast, and heat-affected zones of steel weldments (39);

Annu. Rev. Mater. Res. 2007.37:93-126. Downloaded from arjournals.annualreviews.org
by University of Virginia Libraries on 02/20/08. For personal use only.

bond coats for thermal barrier coatings (TBC) (40); single-crystalline, fully lamellar, and polysynthetically twinned TiAl (41–43); nanocrystalline Ni, Cu, and Al (33, 44, 45); and electron-irradiated 316 stainless steel and Fe-Cu-Mn alloys (46). For example, the microtensile specimen shown in **Figure 1*d*** was electrode discharge machined from a pellet of nanocrystalline Ni with a specially shaped graphite electrode (44). The surfaces and sides of the microsamples were mechanically polished to a mirror finish, using diamond-impregnated papers, Al_2O_3 slurry, and a rotary polishing tool.

Microcompression specimen: mechanical test specimen FIB milled into the surface of a bulk specimen that has a cylindrical geometry with a diameter of less than 100 microns and that is loaded in compression with a modified nanoindenter

The recent emergence of commercial FIB instruments provides a unique opportunity to machine specimens with submicron resolution and damage layers that are much smaller than for traditional machining techniques. Use of a dual-beam FIB with ancillary detectors allows direct viewing of the specimen as it is being shaped and in situ characterization of the region from which the specimen is being taken. This feature, the ability to deposit Pt or W in controlled shapes, the availability of submicron (20–50 nm) ion beams, 3-D stages, and fully automated control capabilities have made the FIB an invaluable tool for fabricating micron-sized structures. Although the FIB can cut with extreme accuracy, the rate of milling must be considered in micromachining applications. Milling rates are material-specific, but rates of 1000 μm^3 min^{-1} are typical, and specimen preparation requires a judicious use of the FIB.

Uchic et al. (47) have pioneered the use of the FIB to fabricate microcompression specimens into the surface of bulk materials (see, for example, **Figure 1*e***). The fabrication of microcompression specimens has several key advantages: The volume of material to be milled is smaller than for microtensile specimens, the microcompression specimens remain attached to the substrate and are easy to handle, the specimens are conveniently loaded with a nanoindenter, and the fabrication of an array of microcompression specimens in the FIB can be scripted and automated. FIB milling rates do limit the rate at which specimens can be made, but specialized femtosecond laser machining and electrode discharge machining, chemical milling, and electropolishing techniques are also being pursued. As a complement to the microcompression specimens, the framed microtensile specimens shown in **Figure 1*f*** have recently been prepared from high-purity Au and Mo single crystals by EDM machining 300-μm-thick specimens with a 50-μm-wide central beam, electropolishing to thin this central section further and to remove any recast layer, and FIB machining a 100-μm-long by 2–40-μm-wide and -thick gauge section into the central section (48; C. Eberl, unpublished research).

Force Application and Measurement

Consider a tensile specimen with a cross section 1 μm by 1 μm and strength of 1 GPa; these are reasonable numbers. The maximum force required to test it is 1 milli-Newton or 0.1-g force, and a resolution of 1–10 micro-Newtons is desirable. Commercial load cells with a range of 5-g force and a resolution of 0.001 g are available and can be used to measure force on such a small specimen. If a specimen can be attached to a load cell, displacement of the other end can be achieved with precision piezoelectric or screw-driven actuators. Overall motion of the movable grip

Annu. Rev. Mater. Res. 2007.37:93-126. Downloaded from arjournals.annualreviews.org
by University of Virginia Libraries on 02/20/08. For personal use only.

can be measured with capacitance probes having a resolution of 10 nm, but compliance of the load train and load cell and localized plasticity in the shoulders of the specimen make it very difficult to estimate strain from measurements of grip displacement. Sharpe et al. (32) describe in detail a system for applying and measuring the forces on a specimen like the one shown in **Figure 1*a***. A similar approach is followed for the narrow specimen of **Figure 1*b*** except that the grip end of the specimen is glued to a 140-μm-diameter silicon carbide fiber with a UV-curing adhesive (49).

Commercial nanoindenters provide subnanometer displacement resolution and a load resolution of 1 nano-Newton. Uchic et al. (47) have shown that a nanoindenter retrofitted with a flat tip is well suited for loading microcompression specimens. A uniform stress field is produced in the gauge section during compression testing. However, compression loading produces unique challenges with regard to alignment, buckling, and end constraints. Zhang et al. (51) have made recommendations regarding allowable aspect ratios, filet radii, and taper, but the importance of substrate constraints and alignment deserves further consideration. These challenges notwithstanding, the fabrication and testing of microcompression testing have spread rapidly.

Annu. Rev. Mater. Res. 2007.37:93-126. Downloaded from arjournals.annualreviews.org
by University of Virginia Libraries on 02/20/08. For personal use only.

Strain Measurement

One cannot simply apply the ubiquitous foil resistance gauge to a microtensile specimen. Attempts to determine strain from grip displacement are complicated by the compliance of the test machine, especially when adhesive is used to mount the specimen. A method for subtracting out the compliance from specimens of different lengths and widths, introduced by Greek & Johansson (52), can be used if the compliances of the specimens are sufficiently different. However, individual uncertainties are additive and lead to twice the scatter, and if possible it is best to measure strain in the gauge of the specimen.

There are other indirect methods of tensile strain measurement. Espinosa et al. (53, 54) create tensile tests by pushing the middle of a long, narrow strip of Au film that is fixed at each end. The vertical deflection along the strip is measured by interferometry and converted into the elongation of the strip. Haque & Saif (55, 56) have constructed a test system that combines the test machine and the specimen into one integral unit, which is mounted in a scanning electron microscope (SEM) and elongated with a piezoelectric actuator. Observations of the relative displacement of two sets of markers enable determination of the force as well as the overall elongation of a very small thin film specimen.

Direct strain measurement at the microscale is a challenge, but there have been several advances in the past ten years. For example, if two reflective markers are placed on a specimen and illuminated with a laser, interference fringe patterns are generated. This is the same as Young's two-slit phenomenon, but in reflection. The fringes move as the specimen is strained, and this motion can be sensed with photodiode arrays and converted into strain on a real-time basis. This noncontact strain measurement method is referred to as the ISDG (57). Suitable markers are shown in **Figure 2**, which shows two pairs of Au lines that were vapor deposited as the last step in the processing of the polysilicon specimen in **Figure 1*a*** (58). This enables measurements

Annu. Rev. Mater. Res. 2007.37:93-126. Downloaded from arjournals.annualreviews.org
by University of Virginia Libraries on 02/20/08. For personal use only.

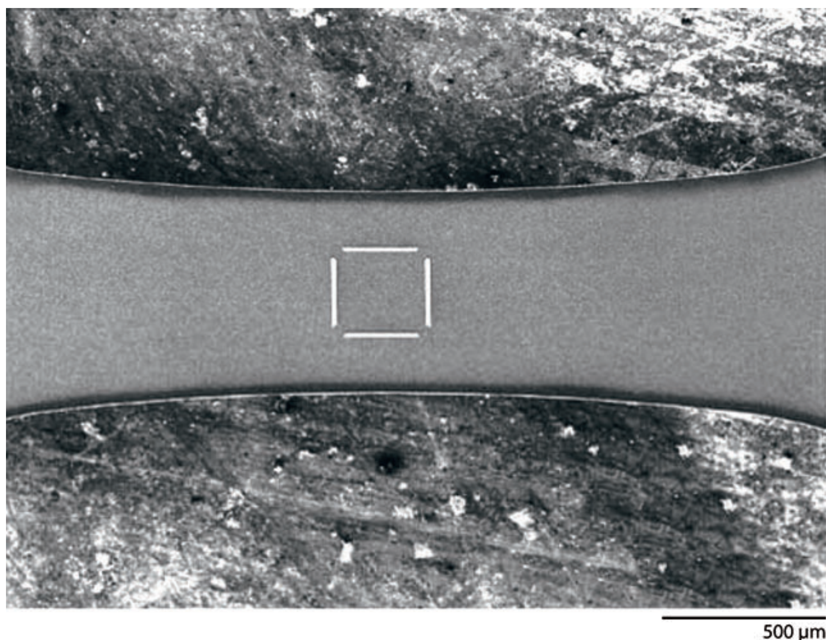

Figure 2

ISDG reflective markers (58). The geometry of these lines is defined by photolithography, and they are deposited by vapor deposition during the manufacturing process. Each line is 0.5 μm high, 20 μm wide, and 200 μm long, and the lines are 300 μm apart.

of transverse strain and therefore of Poisson's ratio. Diamond-shaped microhardness indentations make good reflective markers; they are easier to apply and are used for metallic microtensile specimens like the LIGA specimen shown in **Figure 1*c*** (59). FIB-deposited Pt lines have also proven to be both excellent reflective markers and easy to apply; the ability to image with the FIB facilitates precise placement of the markers.

DIC: digital image correlation

DDIT: differential digital image tracking

A more recent direct method is digital image correlation (DIC). The image can be obtained optically (60–62), in a SEM (63), or from AFM scans (64). This approach is being applied to submicron nanocrystalline Al thin film specimens having the shape of **Figure 1*a***; it not only has the advantage of full-field strain measurement but captures the local shape changes associated with yielding and fracture. A simpler and less computationally intensive method, differential digital image tracking (DDIT), simply tracks two or more markers on a tensile specimen (50). These markers can be either reflective lines applied in processing or ceramic particles held in place by electrostatic attraction. A disadvantage of these methods is that postprocessing is required, which can take from minutes to hours, depending upon the complexity of the patterns. One cannot therefore make in situ full-field strain measurements during a test. However, it is quite reasonable to predict that high-resolution real-time strain measurement by digital image processing will soon be a reality, making digital image processing the predominant method because little or no special surface preparation is required. **Figure 3** shows strain measured on two materials—polysilicon and silicon dioxide—by the ISDG and DDIT, respectively. These are both brittle linear-elastic materials, and the resolution of both techniques is adequate for elastic modulus measurements.

Annu. Rev. Mater. Res. 2007.37:93-126. Downloaded from arjournals.annualreviews.org
by University of Virginia Libraries on 02/20/08. For personal use only.

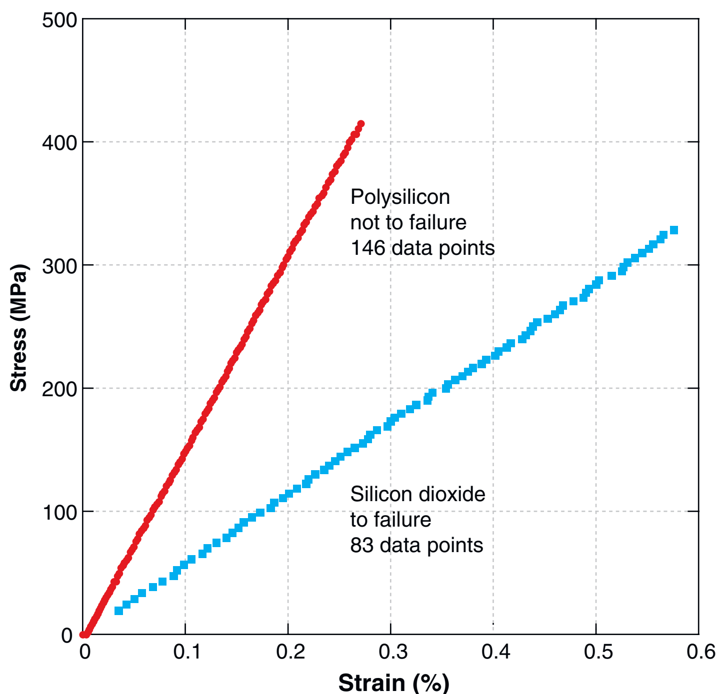

Figure 3

Stress-strain data taken in the elastic region of microtensile tests. The strain data in the polysilicon test were measured using the ISDG, and strain in the silicon dioxide specimen was obtained using DIC. The sharpness of the linear-elastic data sets illustrates the fidelity of these strain measurement techniques (50).

Elevated Temperature Microspecimen Testing

Micromechanical testing at elevated temperatures poses a number of unique challenges. Size restrictions make it difficult to surround the microtensile specimen with a conventional furnace, the load cell and other sensitive components must be thermally isolated from the specimen, and strain measurement is much more problematic because standard methods such as strain gauges and extensometers are not applicable. As described below, these challenges have been overcome for microtensile testing, but elevated temperature microcompression testing has been slower to develop because commercial nanoindenter systems that can be used at elevated temperatures are still under development.

Zupan et al. (65) have shown that bowtie-shaped metallic microtensile specimens can be resistively heated to more than 1100°C, using ~2 volts DC and specially designed self-aligning grips that are thermally and electrically isolated from the load frame (see **Figure 4**). Measurement of the temperature across the microtensile specimen with both thermocouples and an optical pyrometer has verified the absolute temperature of these experiments and shown that temperature gradients in the microtensile specimen are modest (~5°C) in the center of the gauge, where strain is measured with the ISDG system (65). The validity of this technique was further illustrated by the accurate measurement of the Young's modulus (E) and CTE of single-crystalline TiAl at temperatures between 400°C and 1000°C (42). The robustness of this form of microtensile testing has been demonstrated by the measurement

Annu. Rev. Mater. Res. 2007.37:93-126. Downloaded from arjournals.annualreviews.org
by University of Virginia Libraries on 02/20/08. For personal use only.

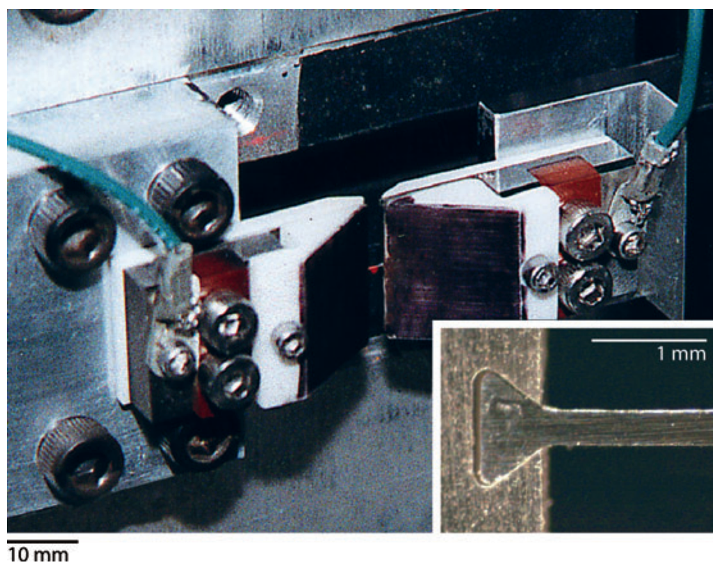

Figure 4

Grips for elevated temperature microtensile experiments. Bowtie-shaped specimens are held in self-aligning grips that are thermally and electrically isolated from the load train. Specimens are heated to more than 1000°C with resistive heating.

of the elevated temperature properties of a wide variety of materials, e.g., single-crystalline and fully lamellar γ-TiAl (41–43); bond coats for thermal barrier coatings (40); LIGA Ni for MEMS (59, 66); high-strength, high-conductivity Cu alloys (67); and $\alpha + \beta$ Ti alloys (68).

Elevated temperature strain measurement can be accomplished with the noncontact ISDG if suitable reflective markers can be placed in the gauge of the specimens. Microhardness indents work well for thicker metallic specimens but cannot be used on extremely thin or brittle specimens. Lithographically deposited Au lines work well at room temperature but diffuse into polysilicon at approximately 200°C. By contrast, Pt lines are much more robust and can easily be written onto the specimen with a FIB. Digital imaging is an attractive alternative to the ISDG because it can use less perfect markers for either correlation or tracking, but special care and lighting must be employed to assure that the image is not washed out by distortions due to convective flow or the glow of the specimen at high temperatures. In all cases, one must be careful of oxidation; the Au and Pt lines themselves will not oxidize, but surface oxides can easily overwhelm these indents and submicron lines. Oxidation-resistant specimens or environmental control may be required.

The use of elevated temperature microtensile testing is not limited to metallic materials. Polysilicon is a semiconducting material whose resistivity depends on doping; commercial specimens like the one in **Figure 1*a*** have resistances on the order of 40–60 ohms and can be heated to 800°C with less than 10 volts DC (69). The planar shape of the specimen with gentle curvature into the center concentrates the temperature rise there over a length of 300 μm, as shown in **Figure 5**, and allows a room temperature test machine to be used without modification.

The smaller specimens of **Figure 1*b*** have been heated to 200°C in a small furnace consisting of a resistively heated block on the back side and a quartz window on

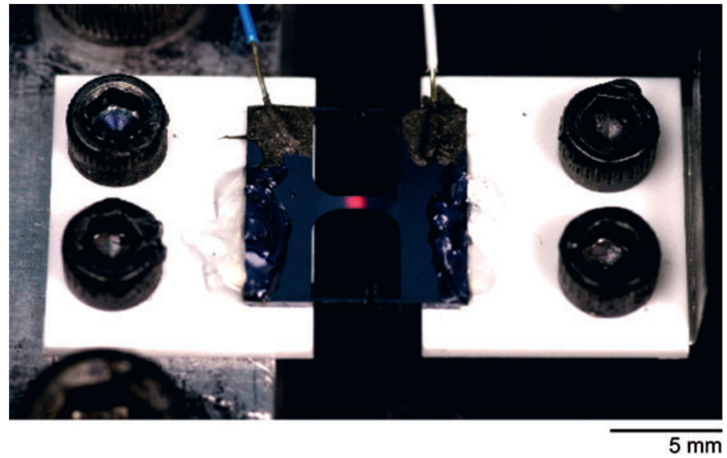

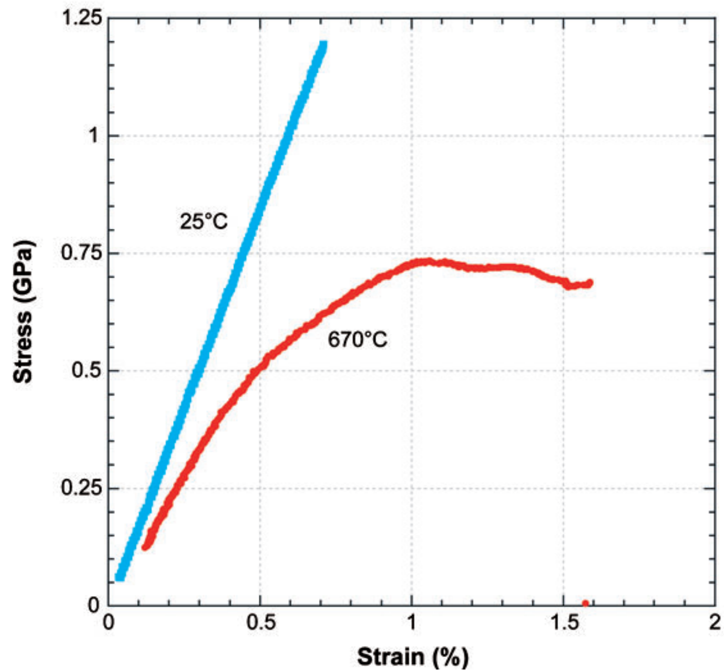

Figure 5

(*Top*) A resistively heated and glowing polysilicon microtensile sample in the grips and ready to be tested. (*Bottom*) Stress-strain curves obtained at 25°C and 670°C (69).

Annu. Rev. Mater. Res. 2007.37:93-126. Downloaded from arjournals.annualreviews.org
by University of Virginia Libraries on 02/20/08. For personal use only.

the front to allow optical access for strain measurement (70). Silicon carbide has potential for use in MEMS, but it is extremely difficult to micromachine. Various manufacturing processes are under development, and the strength of microtensile specimens is being used to judge the efficacy of these processes. The strength of silicon carbide microtensile specimens has been measured at 1000°C with a modified commercial furnace and the specially shaped ceramic grips shown in **Figure 6** (38). The upper grip is fixed to a ceramic rod extending up through the bottom of the

Annu. Rev. Mater. Res. 2007.37:93-126. Downloaded from arjournals.annualreviews.org
by University of Virginia Libraries on 02/20/08. For personal use only.

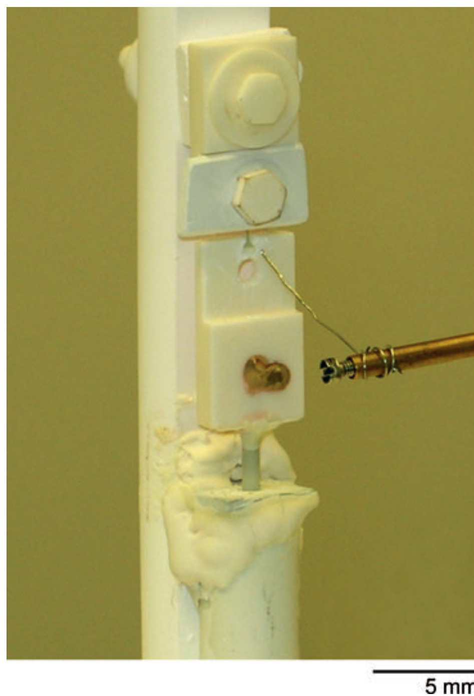

Figure 6

A silicon carbide microtensile specimen in the inserts of ceramic grips. The wire on the end of the micromanipulator is used to seat the specimen in the grips (38).

furnace. The lower movable grip is attached to a long nichrome wire that is enclosed in a small ceramic tube to prevent oxidation and connected to a load cell and translation stage that are positioned under the furnace, out of the hot zone.

SIZE EFFECTS ON MECHANICAL BEHAVIOR

Until recently, for both engineering components and tensile specimens, the external dimensions were larger than the internal microstructural features, and the importance of external size effects on mechanical properties could safely be ignored. The development of microelectronic thin films, advanced coatings, MEMS, and nanoelectromechanical systems (NEMS) has resulted in components with sizes approaching microstructural dimensions, and external size effects have become increasingly more important. The testing of microspecimens offers a direct avenue for mimicking and measuring the mechanical size effects associated with these small-scale structures. Efforts to design and model the reliability of small-scale devices are directly dependent on the availability of accurate and reliable "handbook" values of the elastic, plastic, fracture, and fatigue properties of materials at relevant length scales. Developing a fundamental understanding of these external size effects will not only allow for better design of small-scale devices but also provide a much-needed foundation

NEMS: nanoelectromechanical systems

for developing multiscale models of complex structural materials. Such models are based on the mechanical behavior of individual microstructural entities, which can best be measured and understood using the types of experiments outlined in this paper. The first half of this paper focuses on the challenges and techniques associated with microscale testing; this section highlights the results of recent microscale experiments and provides a snapshot of our understanding, to date, of size effects on the mechanical behavior of these structures.

Elastic Response

The difficulty associated with measuring mechanical properties with microspecimens is clearly illustrated by the recent evolution in the published values of the Young's modulus for polysilicon, which burst onto the MEMS scene in the late 1980s. The isotropic elastic constants (E and ν) of polysilicon are needed for accurate component design. However, there is no bulk counterpart to provide a guide; polysilicon exists in bulk form, but its microstructure is very different than what is produced by vapor deposition. Consequently, numerous groups undertook studies to measure the Young's modulus of polysilicon. **Figure 7** shows the range in the published values of Young's modulus as a function of year. The wide scatter in the early data is surprising, and the convergence that occurred over a relatively short four-year period is noteworthy. The early scatter in the data is associated with inaccuracies in testing methodologies. For example, measurements that suggested that Young's modulus decreases for micron-sized specimens were found to be influenced by the fact that undercutting during etching led to errors in sample geometry (71).

A generally accepted value for the Young's modulus of polysilicon is now 160–165 GPa; see, for example **Figure 8**, which shows the stress-strain curves taken from

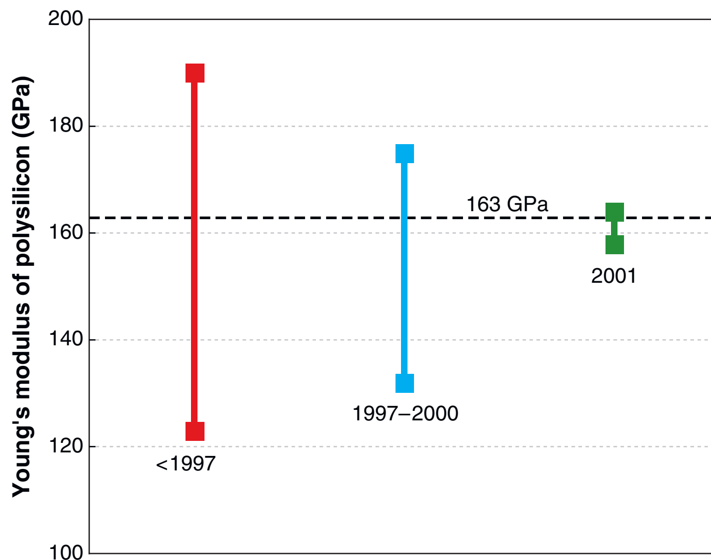

Figure 7

The spread in the published values for the Young's modulus of polysilicon given as a function of year. The wide variation in early measurements is believed to be associated with the use of unreliable testing methodologies, but it is encouraging that the convergence in measured values observed in 2001 agrees with calculations of the in-plane elastic modulus (163 GPa) (*black horizontal line*) based on anisotropic elasticity.

Annu. Rev. Mater. Res. 2007.37:93-126. Downloaded from arjournals.annualreviews.org by University of Virginia Libraries on 02/20/08. For personal use only.

Annu. Rev. Mater. Res. 2007.37:93-126. Downloaded from arjournals.annualreviews.org
by University of Virginia Libraries on 02/20/08. For personal use only.

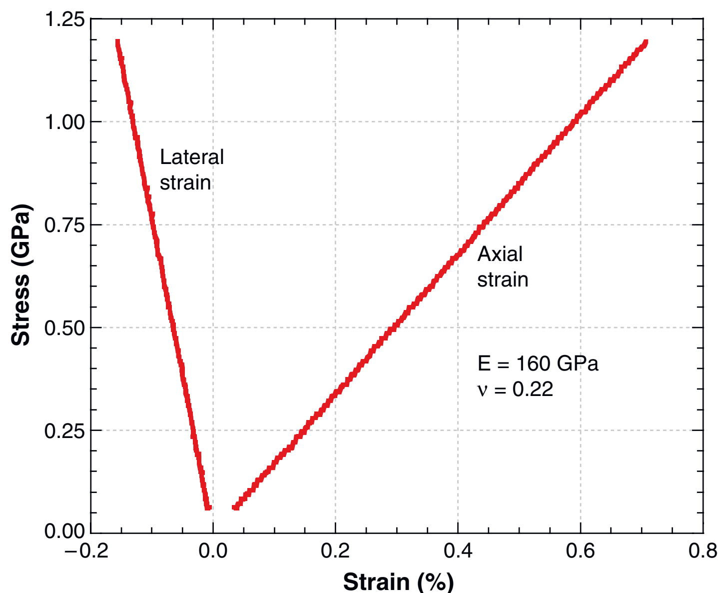

Figure 8

A plot of stress verses axial and lateral strain as measured by ISDG on freestanding polysilicon specimens like those in **Figure 1*a***. Availability of both axial and lateral strain allows for the determination of Poisson's ratio (ν) as well as Young's modulus (E) (72).

a microtensile experiment performed on a framed specimen like the one shown in **Figure 1*a*** (72). The axial and lateral strain was measured by the ISDG and used to calculate the elastic constants (E = 160 GPa and ν = 0.22). These values are almost the same as those obtained by bulge testing (E = 162 ± 4 GPa and ν = 0.2 ± 0.03) (26). Hashin-Shtrikman bounds of the in-plane elastic moduli that were calculated on the basis of anisotropic elasticity, ⟨110⟩ crystallographic texture, and the stiffness matrix for single-crystalline Si give values (E = 163.0–165.5 GPa and ν = 0.22–0.24) that are in good agreement with these experimental results (26).

The elastic constants of 3C polycrystalline silicon carbide thin films have also been measured using framed microtensile specimens with geometry similar to the one shown in **Figure 1*a*** (73). These specimens ranged from 20–40 μm thick and were prepared by deposition into molds cut into a Si wafer by DRIE. The front side of each specimen was laboriously hand-polished to remove the overflow from deposition, and a back-side window was etched with XeF_2. As was found for polysilicon, the measured in-plane elastic constants (E = 448 ± 13 GPa and ν = 0.17) were consistent with calculations of Voight and Reuss averages based on single-crystal constants (E = 441–460 GPa). Thinner single-crystalline films were epitaxially grown on (100) Si wafers, and identically shaped ⟨110⟩-oriented microtensile specimens were prepared by micromolding and by reactive ion etching (RIE) (75). The measured value of $E_{\langle 110 \rangle}$ was 424 ± 44 GPa, which is similar to but a little lower than the value predicted by anisotropic elasticity (455 GPa).

A recent comparison of elastic measurements by tensile testing and bulge testing showed excellent agreement (27). In this study, silicon nitride films 0.5 μm thick were deposited onto a Si wafer and both microtensile specimens, as in **Figure 1*a***, and 1-mm-square membranes were released from the back. The latter were bulge tested

at Exponent, Inc. in a setup that recorded the full-field membrane deformation by optical interferometry. Independent measures of Young's modulus were obtained from both tests; the microtensile tests yielded 257 $\pm$ 5 GPa, and the bulge tests, 258 $\pm$ 1 GPa. This startling agreement confirms both test methodologies.

Electrodeposited LIGA Ni bowtie-shaped microtensile samples, like the one shown in **Figure 1*c***, were initially measured to have a Young's modulus of approximately 180 GPa, which is significantly lower than the bulk value for polycrystalline Ni (207 GPa). This value, however, can be explained and modeled in terms of the strong $\langle 001 \rangle$ out-of-plane texture in these electrodeposited Ni specimens (35). Subsequent investigations have shown that the Young's modulus of weakly $\langle 110 \rangle$ textured LIGA Ni microtensile specimens is 204 GPa and that variations in specimen texture lead to variations in experimentally measured modulus that are in good agreement with the values predicted by averages of the anisotropic stiffness matrix for single-crystalline Ni (76).

Taken together, the microtensile measurements on MEMS polysilicon, silicon carbide, silicon nitride, and LIGA Ni (*a*) indicate that variations in crystallographic texture may lead to differences in Young's modulus but (*b*) affirm the fact that the fundamental elastic response is not altered by having micron-sized specimens. The latter finding is not surprising, as elasticity is a material property that depends on atomic bonding.

Microtensile samples similar to those shown in **Figure 1*c*** have been cut from single-crystalline TiAl and tested at temperatures ranging from 400°C to 1000°C (42). The modulus was the same along [100] and [010], was significantly stiffer along [−110], and fell gradually with temperature for all orientations (**Figure 9**). These microsample data were in very good agreement with extrapolations of the modulus obtained using resonant ultrasound spectroscopy of centimeter-sized crystals (77). Similar microtensile experiments on specimens of diffusion aluminide bond coats for thermal barrier coatings (40) and a high-strength, high-conductivity Cu alloy, GRCop-84 (67), have also produced values of E that are in agreement with bulk values of these alloys. In general, moduli obtained from microtensile samples with dimension of hundreds of microns have been found to be the same as those obtained using more traditional macroscale specimens.

The situation appears to be different for very thin films of vapor-deposited pure metals. Huang & Spaepen (78) have summarized microtensile measurements of vapor-deposited metallic thin films with thickness of several microns and reported that the stiffness of both pure films and multilayers was on average 10–20% below what is predicted from averages of the anisotropic elastic constants. Similarly, recent measurements made using microspecimens of vapor-deposited Au place E between 35 GPa and 88 GPa (79); most values are at approximately 50 GPa (54), which is considerably lower than the value of 80 GPa that is typically reported for bulk specimens. Haque & Saif (56, 80) have also reported moduli taken from 30–50-nm-thick freestanding Au and Al films that were significantly below their bulk values, and they attributed this decrement to grain boundary compliance and the presence of an amorphous grain boundary phase. HREM observations of nanocrystalline grains indicate that they are crystalline all the way to the boundary (81, 82). Huang & Spaepen (78)

Annu. Rev. Mater. Res. 2007.37:93-126. Downloaded from arjournals.annualreviews.org
by University of Virginia Libraries on 02/20/08. For personal use only.

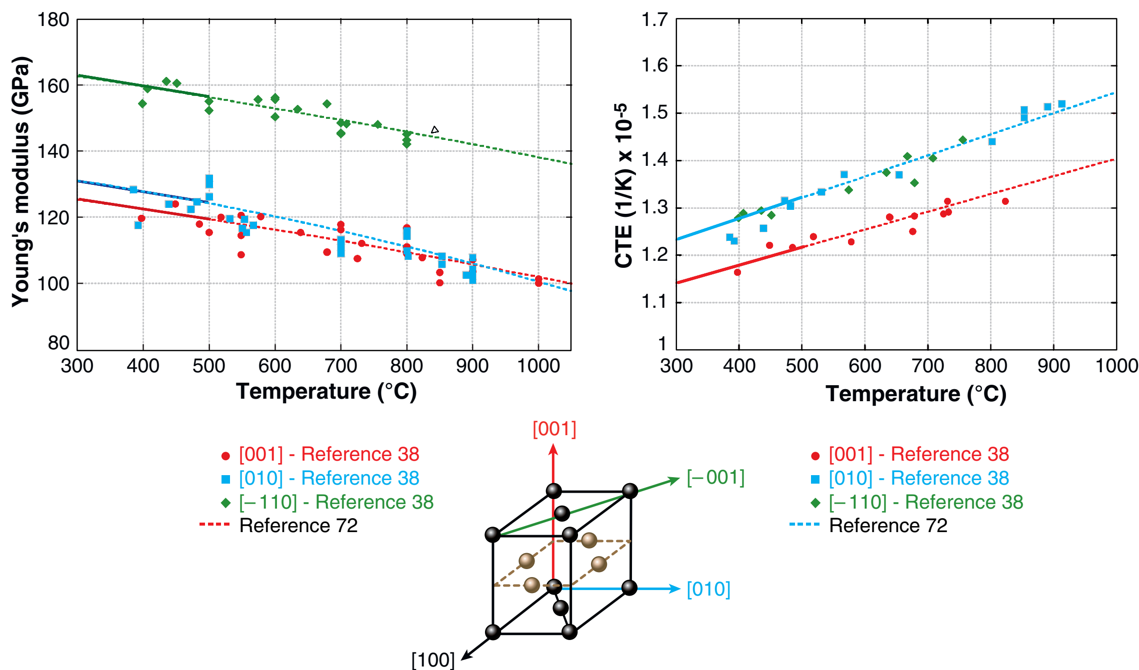

Figure 9

Microtensile measurements of E and CTE for γ-TiAl single crystals at three different orientations and as a function of temperature (42). The solid lines are based on experimental ultrasound measurements of bulk crystals (77), and the dashed lines are extrapolations of those data. The microtensile data are in excellent agreement with both and clearly extend the range over which data can be collected.

considered and discounted the influence of crystallographic texture, voids, microplasticity, anelasticity, and compliant grain boundaries and concluded that the increased compliance was related to the presence of microcracks in the grain boundaries between the columnar grains of vapor-deposited materials. Recent TEM observations of sputter-deposited Au thin films that exhibit a reduced modulus of approximately 50 GPa provide evidence of elongated grain boundary voids that could result in microcracking (79).

Strength of Brittle Materials

Many MEMS materials are brittle at room temperature and exhibit linear elastic behavior up to the point at which they fracture. The fracture strength of brittle materials is determined by the distribution of flaws on the surface or interior of a component and by the fracture toughness of that material. For a brittle material with a random distribution of flaws, a smaller area or volume will likely have fewer large flaws that lead to failure; therefore, smaller specimens or stressed regions tend to have higher fracture strengths. Tension tests of polysilicon demonstrate this size effect, as

Annu. Rev. Mater. Res. 2007.37:93-126. Downloaded from arjournals.annualreviews.org
by University of Virginia Libraries on 02/20/08. For personal use only.

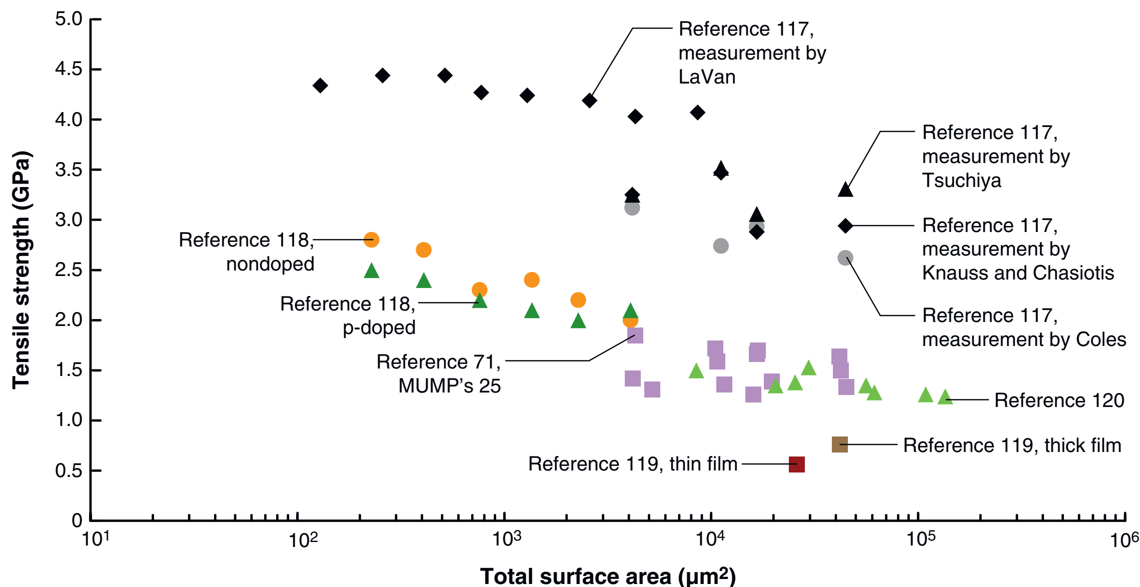

Figure 10

Fracture strength of polysilicon in terms of total surface area of the specimen (84).

is indicated in **Figure 10**, which shows fracture strengths from several sources plotted as a function of the total surface area of the gauge section (84). Even though these specimens were made in different MEMS foundries and tested with different tensile test methods, the trend is clear; decreasing the total surface area increases the fracture strength of the specimen.

The importance of surface defects in determining the fracture strength of polysilicon is further illustrated by results collected at Johns Hopkins University on specimens that were provided by three different collaborators. More than 100 tests were conducted, and the mean strength of the specimens made by the MUMPS process was 1.6 GPa; in contrast, those made at SMI Inc. failed at 2.0 GPa, and the specimens made at Sandia National Laboratories exhibited strengths of 3.1 GPa (85). TEM examination of these specimens discounted internal microstructural effects, and the difference in strength has been attributed to observed variations in side-wall roughness, which corresponds to differences in processing. Chasiotis & Knauss (86), who compared MUMPS polysilicon with Sandia polysilicon, obtained similar results and arrived at the same conclusions.

This dependence of fracture strength on surface roughness can explain an apparent contradiction in the use of polysilicon as a structural material for MEMS devices. Very few, if any, large load-bearing structures are made of Si. Its inherent brittleness at room temperature and low fracture toughness are seen as clear impediments to its use as a macroscopic structural material. In that light, it is curious that the use of polysilicon for microscale devices is extremely widespread; more MEMS devices

Annu. Rev. Mater. Res. 2007.37:93-126. Downloaded from arjournals.annualreviews.org by University of Virginia Libraries on 02/20/08. For personal use only.

are made out of polysilicon than any other material. This apparent paradox can be explained by considering the Griffith relation between fracture strength and flaw size. Ballarini and colleagues (87, 88) have shown that the fracture toughness of Si ($1\ MPa\sqrt{m}$) is independent of its microstructure and essentially the same for amorphous Si, polysilicon, and single-crystalline Si. MEMS flaws are typically submicron, whereas macro structures contain flaws that are more aptly described as submillimeter. For a constant fracture toughness of $1\ MPa\sqrt{m}$, the simplest form of the Griffith relation ($K_{IC} = \sigma_f \sqrt{\pi a_o}$) predicts a fracture strength of approximately 20 MPa for a macrostructure with a flaw size (a_o) of 0.5 mm and more than 500 MPa for MEMS structures with flaw sizes of 0.5 μm. It follows that allowable stresses for MEMS polysilicon are substantially higher because the flaws are so much smaller.

Namazu et al. (89) also convincingly demonstrated the influence of specimen size in determining fracture strength for single-crystalline Si. These researchers tested cantilever beams with widths, thicknesses, and lengths as small as 0.20 μm by 0.26 μm by 6 μm and larger specimens with dimensions up to 1.0 mm by 0.5 mm by 9.8 mm. The fracture strength was computed from the measured force applied at the end of the cantilever; this was determined with an atomic force microscope (AFM) probe for the smaller specimens and by more conventional means for the larger ones. Namazu et al. (89) report an increase in fracture strength from 0.47 GPa for the largest specimen to 17.5 GPa for the smallest, an astonishing 37-factor increase.

The strength of micromolded 3C polycrystalline silicon carbide is also size dependent, although the influence of size on strength is not as dramatic as for single-crystalline Si. The framed microtensile specimens used to determine the elastic constants were pulled to failure, and thicker micromolded specimens had an average strength of 0.81 ± 0.23 GPa (69, 70). In contrast, thinner micromolded ones failed at 1.19 ± 0.53 GPa (75). The effect of processing was also evident in this study, as thicker RIE specimens were measured to have an even higher strength of 1.65 ± 0.39 GPa (75).

Thicker specimens with the overall bowtie shape of **Figure 1*c*** and well-defined stress concentrations, notches, or holes designed into the gauge section were etched from 150-μm-thick commercial silicon carbide wafers. Microtensile specimens with smooth gauge sections were used to obtain baseline values, and stress concentration factors were used to determine the fracture strength of the notched specimens. The average fracture strengths (computed via the stress concentration factors) were 0.47 ± 0.39 GPa for the smooth gauge specimens and 0.78 ± 0.28 GPa for the notched ones (90). The difference in these values can be attributed to the difference in the volume of material that is stressed. Detailed fractographic analyses showed failures initiating at the bottoms of side grooves left by the etching process. Single-crystal specimens with holes instead of notches were tested at room temperature and 1000°C and showed slightly higher values but the same trend (38). The average room temperature fracture strength of the smooth specimens was measured to be 0.66 ± 0.12 GPa, whereas the specimens with the circular hole failed at 1.24 ± 0.34 GPa. Almost identical values were obtained at 1000°C. From these results, one can conclude that (*a*) the fracture strength of silicon carbide exhibits a size effect,

Annu. Rev. Mater. Res. 2007.37:93-126. Downloaded from arjournals.annualreviews.org
by University of Virginia Libraries on 02/20/08. For personal use only.

(*b*) fabrication processes have a strong effect on this strength, and (*c*) testing small brittle specimens that are difficult to manufacture leads to a high coefficient of variation (COV).

Taken at first blush, microtensile measurements of size-scale effects on the strength of brittle materials are best represented by variations in flaw size and distribution; at the atomic scale the physics of fracture remains the same. Surface flaws dominate and appear to be much more important than internal microstructure, and the significance of processing in determining side-wall roughness cannot be overstated.

Strength of Ductile Materials

The yield strengths of ductile materials are governed by intrinsic processes that facilitate microplasticity and are fundamentally different than the atomic mechanisms associated with brittle crack propagation. In most cases, the strength of ductile materials is closely related to the stress required to move dislocations past obstacles and is not nearly as dependent on the presence of flaws. In this light, it is worth reviewing the role that both intrinsic and extrinsic size effects have on dislocation activity and the resultant plastic deformation that occurs in metals and alloys.

Intrinsic size effects. Not all MEMS materials are brittle; electrodeposited LIGA metallic structures offer a broad range of mechanical properties. To date, the majority of LIGA structures have been fabricated with electrodeposited Ni, and microtensile experiments have shown that LIGA Ni possesses good strength and considerable tensile ductility (59, 66); see, for example, the stress-strain curves in **Figure 11**, which were obtained using bowtie-shaped specimens like the one shown in **Figure 1*c***. The curves in **Figure 11** were obtained from specimens that were deposited using different current densities, and they illustrate how small, often unintentional variations in electrodeposition parameters can lead to significant property variations. The dramatic increase in strength shown in **Figure 11** is the result of the decrease in grain size associated with lower current densities. Thermal instabilities, primarily grain growth, reduce the strength of LIGA Ni at temperatures as low as 200°C (59, 66), and efforts to stabilize the microstructure with alloying and dispersions are receiving increased attention.

The example given above is not an isolated one, as the deposition of metals in MEMS and other thin film applications often naturally results in nanocrystalline microstructures. Microtensile tests have proven to be useful for characterizing the mechanical behavior of nanocrystalline metals (see Reference 92 for a review). These studies all point to a concomitant increase in strength and loss of ductility associated with diminishing grain size. There is general recognition that normal dislocation activity is inhibited at grain sizes below approximately 50 nm, and the emerging view is that the ductility of nanocrystalline metals is limited by a lack of dislocation multiplication and the required operation of less efficient deformation processes. Molecular dynamics simulations suggest that nanocrystalline metals accommodate external loads through grain boundary sliding and the emission of unit and partial dislocations that traverse the grain and are absorbed into the opposite grain boundary

Annu. Rev. Mater. Res. 2007.37:93-126. Downloaded from arjournals.annualreviews.org
by University of Virginia Libraries on 02/20/08. For personal use only.

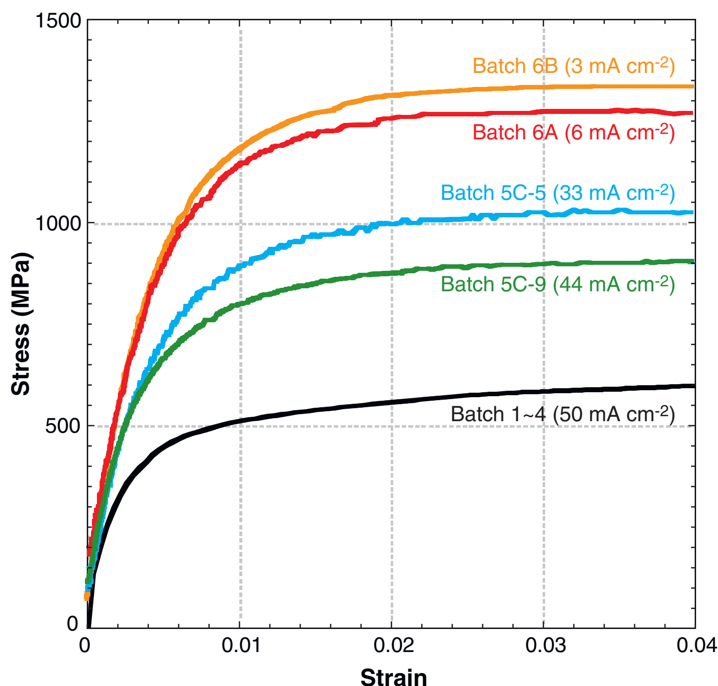

Figure 11

The stress-strain response of electrodeposited LIGA Ni microtensile specimens. Unexpected batch-to-batch variations in the flow behavior have been traced to changes in plating current density, which leads to changes in crystallographic texture and greatly reduced grain sizes. Current densities of 50 mA cm^{-2} produced specimens with a strong ⟨001⟩ out-of-plane texture and an average grain size of 4 μm, whereas 6 mA cm^{-2} resulted in a weak ⟨011⟩ texture and heavily twinned 200-nm grains. Young's modulus varied with crystallographic texture, whereas the yield strength of these specimens showed a Hall-Petch dependence on grain size. The dramatic increase in strength measured in these specimens is associated with the formation of nanocrystalline specimens.

Annu. Rev. Mater. Res. 2007.37:93-126. Downloaded from arjournals.annualreviews.org
by University of Virginia Libraries on 02/20/08. For personal use only.

without multiplying or interacting with other dislocations (93–96). The prediction of partial dislocation emission is supported by TEM observations of deformation twinning and stacking fault formation in nanocrystalline Al (81). The overall picture is consistent with post-mortem TEM observations (44, 97) and in situ X-ray diffraction experiments (98), which indicate that permanent dislocation networks are not built up during plastic deformation.

Descriptions of room temperature deformation in nanocrystalline metals have generally considered their microstructures to be stable, but emerging evidence suggests that the mechanical behavior of these structures is not only different than that of microcrystalline metals but dynamic as well. Rapid grain growth has been observed at room temperature (33, 99, 100) and in the absence of thermal activation (cryogenic temperatures) (101). Gianola et al. (33) have measured the mechanical response of 100–300-nm-thick nanocrystalline Al films, using framed specimens similar to those

Annu. Rev. Mater. Res. 2007.37:93-126. Downloaded from arjournals.annualreviews.org
by University of Virginia Libraries on 02/20/08. For personal use only.

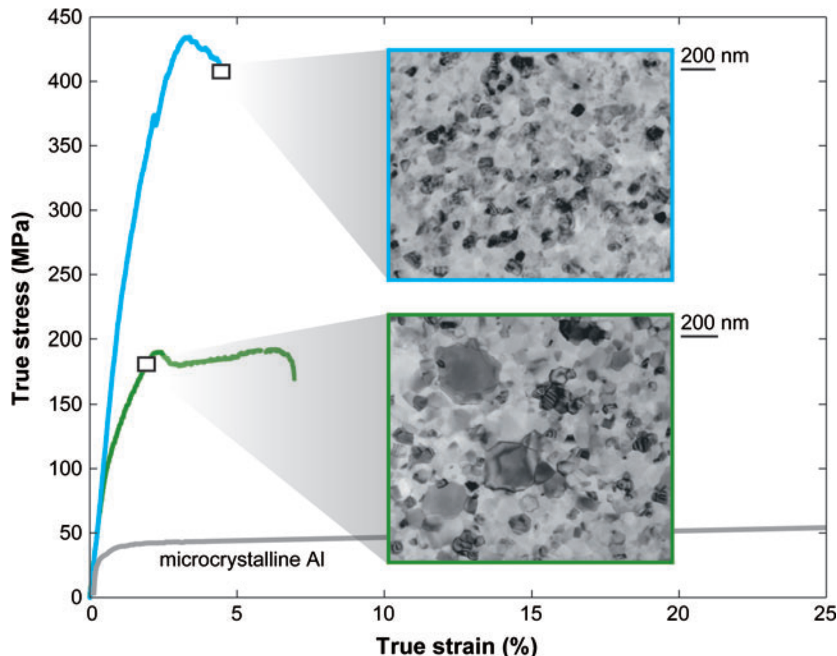

Figure 12

Microtensile stress-strain curves for submicron nanocrystalline Al thin films showing two different types of behavior. The curve with the highest strength, gradual deviation from plasticity, and limited ductility is representative of a specimen that maintains its nanocrystalline grain size. By contrast, specimens observed to undergo stress-assisted room temperature grain growth exhibit lower yield strength, more pronounced deviation from linear elasticity, and regions of extended plasticity. Although not shown here, plastic strains of 40–50% have been observed (33).

shown in **Figure 1*a***. The process flow for these specimens is described above (see section on Microspecimen Preparation and Handling). The tests of Gianola et al. (33) indicate two distinct types of response; representative curves of each are shown in **Figure 12**. Microtensile specimens that maintain their nanocrystalline microstructure exhibit strengths 15–20 times higher than that of coarse-grained Al, gradual deviation from elastic behavior in the early stages of plastic deformation, and limited elongation. By contrast, specimens that undergo discontinuous grain growth show intermediate strengths, more pronounced deviation from linear elasticity, and the unexpected development of a region of extended plasticity. The grain growth was a direct result of the applied stress, and its effect on the mechanical response of these films is unmistakable. Efforts to model this growth with traditional driving forces have proven less than satisfactory, and the importance of grain boundary pinning and the role of stress-assisted room temperature grain boundary migration, similar to that observed by Winning et al. (102, 103) and described by Cahn et al. (104, 105, 106), appear important (33).

In addition to grain boundary strengthening, the size effects of other intrinsic microstructural features (e.g., laths, growth twins, precipitates, and dispersions) are well known and have been studied and discussed extensively; see, for example, the review by Arzt (107). Their behavior in microscale components is the same as in bulk materials as long as the salient microstructural features are smaller than the size of the component. Other, interesting size effects are observed when the dimensions of a component are reduced below that of the microstructure and the distance over which deformation mechanisms operate.

Extrinsic size effects. Extrinsic size effects in dislocation-mediated plasticity are often classified into two types. One class involves the development of mesoscopic plastic strain gradients, and the other occurs when external surfaces or boundary layers interfere with and alter the underlying deformation process.

The importance of strain gradients has been documented by microscale measurements illustrating the fact that many materials are stronger when subjected to nonuniform deformation [e.g., torsion (108), bending (109), or indentation (110)] than they are when uniaxially loaded. The strength enhancement observed in these experiments is generally attributed to the storage of geometrically necessary dislocations, which are associated with strain gradients. The constitutive models associated with classical plasticity theories do not account for this observed strengthening, but Fleck et al. (108) have suggested a phenomenological description of strain gradient plasticity that accounts for both rotation and stretch gradients and provides an internal length parameter that can be used to connect continuum level models with microscale strain gradients. Physical descriptions of this internal length parameter have proven illusive. However, an alternative mechanism-based theory for strain gradient plasticity, which incorporates a Taylor-like description of dislocation interactions and assumes that the flow stress increases linearly with the density of geometrically necessary dislocations, has also been proposed and used to model experimentally measured indentation size effects (13–15).

Uchic and colleagues (47) have developed a unique test platform to explore specimen size effects in bulk materials by employing a FIB to machine cylindrical compression samples into the surface of bulk crystals, as shown in **Figure 1*e***. Samples with diameters of 0.5–40 μm and aspect ratios of 2:1 to 4:1 are tested in compression, using a nanoindenter with a flat tip and strain rates of 10^{-3}–10^{-4} 1 s^{-1}. The results of microcompression experiments on single-crystalline Ni, Ni_3Al, and a Ni-base superalloy point to the effect of free surfaces on the mechanical response of these materials. Curves for the 20–40-μm Ni specimens were similar to those for bulk samples, but smaller specimens displayed large strain bursts and considerably higher flow strengths. Size-scale effects were even more dramatic in the experiments conducted on Ni_3Al, for which strength increased from 250 MPa to 2 GPa. By contrast, the microcompression data for experiments conducted on a Ni-base superalloy were mediated by the underlying microstructure, which contains very fine γ' precipitates that provide internal strengthening and preempt the influence of the external dimensions.

Greer et al. (111) have reported a dramatic increase in the compressive strength of Au micropillars with submicron pillar diameters. Their results on specimens made by both FIB machining and electrodeposition followed by postdeposition heat treatment indicate that this strength enhancement is not an artifact of the specimen preparation processes. Similar to the picture emerging for nanocrystalline materials, Greer et al. interpret their results to be an indication of dislocation starvation unique to small crystals. In these experiments, the dislocations are believed to run to the specimen free surface and out of the crystal before they have an opportunity to interact and multiply. Volkert & Lilleodden (112) have also measured size-scale effects in submicron Au columns and attributed their results to source-limited behavior in

Annu. Rev. Mater. Res. 2007.37:93-126. Downloaded from arjournals.annualreviews.org
by University of Virginia Libraries on 02/20/08. For personal use only.

small volumes. Dimiduk and colleagues (113) have further suggested that the observed size-dependent flow response of single-phase metals is dominated by three stochastic effects: dislocation generation by a stress-dependent source distribution, dislocation escape at free surfaces, and dislocation trapping that changes both the stress-dependent mobile density and source density. This finding holds an important implication for strain gradient plasticity theories. Dimiduk and colleagues (113) point out that if dislocation behavior is stochastic in single-phase metals for characteristic dimensions below ∼20 μm, then size-affected changes in dislocation mechanisms may be more important than gradient-induced storage of geometrically necessary dislocations.

Microtensile complements to these microcompression experiments are more difficult to conduct but are beginning to emerge. Espinosa et al. (54) employed membrane deflection experiments to obtain stress-strain curves of freestanding vapor-deposited submicron films of Au, Al, and Cu and reported that the strength of these films increases with increasing width and decreasing thickness. The dependence of grain size on thickness in vapor-deposited films has been noted by numerous investigators (see for example References 6 and 33) and may complicate the separation of grain size and thickness effects. Recently obtained microtensile tests conducted on specimens prepared from bulk single crystals of Au and Mo and with the geometry shown in **Figure 1*e*** also support the microcompression results (C. Eberl, unpublished research). Reducing the gauge diameter of Mo from 20 to 3 μm increased the ultimate strength from 290 to 550 MPa. Moreover, SEM observations of the surfaces of Au specimens show a transition from smooth to discrete slip, with an increased amount of localized shear deformation in the necked region of the smallest samples. The Mo specimens show evidence of shear localization but no discrete slip steps at the surface, suggesting a fundamental difference between fcc and bcc metals.

Size effects related to the presence of boundary layers are prevalent in the thin films literature. For example, Venkatraman & Bravman (114) measured the strength of Al thin films on a Si substrate with wafer curvature experiments and illustrated that the strength of the film scales with inverse thickness with successive etch back steps. Nix (115) proposed a model for this thickness effect that envisions the bowing of a dislocation between the underlying substrate and an overlying passivation layer and involves the laying out of dislocations along the film-substrate and film-oxide interfaces. More detailed extensions of this model and numerous comparisons with experimental measurements have been forthcoming; see Reference 17 for a review.

Vlassak and coworkers (22, 23) have used a plane-strain bulge testing technique to deform substrate-free films alternatively in tension and compression. Their experiments on electroplated and sputter-deposited Cu films showed that passivated films are significantly stronger than unpassivated films and unveiled a strong Bauchinger effect that increases with prestrain for the passivated films (22, 116). These results have been compared with discrete dislocation (DD) plasticity simulations (25) that allow for both dislocation exhaustion and strain hardening and reproduce the trends found in the experiments. In addition to capturing the Bauschinger effect for passivated films, the DD simulations suggest that, whereas the flow stress of unpassivated films with sufficiently large grains is independent of thickness, the flow stress of very

Annu. Rev. Mater. Res. 2007.37:93-126. Downloaded from arjournals.annualreviews.org
by University of Virginia Libraries on 02/20/08. For personal use only.

thin unpassivated films and films passivated on at least one side does show an h^{-1} dependence on thickness.

Taken as a whole, the studies outlined in this section indicate that there is an intermediate size regime, larger than whiskers and smaller than bulk materials, for which external size effects play an important role in determining mechanical behavior. This effect is often regulated by the refined microstructure in commercial alloys, but for pure metals and single-phase alloys this regime occurs at length scales that are surprisingly large. The interplay between the underlying deformation processes, namely dislocation plasticity, and the mesoscale volumetric constraints, whether they are nanometer-sized grains or micrometer-sized specimens, that govern mechanical behavior at these length scales is still coming into focus. Discerning experimental studies and fundamental theories that describe heterogeneous dislocation nucleation, evolution, storage, and exhaustion are needed. The availability of microscale testing techniques and advanced materials modeling makes this a rich and exciting area for future studies.

Annu. Rev. Mater. Res. 2007.37:93-126. Downloaded from arjournals.annualreviews.org
by University of Virginia Libraries on 02/20/08. For personal use only.

CONCLUDING REMARKS

The emergence of MEMS technologies and availability of microscale processing techniques for making and shaping micron-sized specimens combined with increasingly finer techniques for manipulation, loading, and strain measurement have empowered experimentalists with the ability to probe the mechanical response of increasingly smaller volumes of materials. This trend toward smaller length scales will undoubtedly continue. This review does not report on the absolute smallest tests or purport to be a comprehensive overview of all microscale techniques but rather emphasizes recent developments in the extension of standard uniaxial tension and compression testing to the microscale. Challenges to microscale testing notwithstanding, these tests are easiest and most straightforward to interpret, and clear trends are beginning to emerge to provide a basis for understanding and modeling mechanical behavior at this scale.

Challenges in microscale fabrication are being addressed with both additive and subtractive processes. Techniques such as photolithography, vapor deposition, RIE, LIGA, and electroplating are available in MEMS foundries and can be used to fabricate micro test specimens as well as micro devices. Traditional machining processes are not applicable, but specialty EDM, laser machining, chemical mechanical polishing, and FIB milling may be used to create microspecimens from bulk materials. Underlying substrates and frame geometries facilitate handling and piezo stages loading. Grip displacement does not provide an accurate measure of strain, but very promising noncontact optical techniques have emerged in recent years. The full stress-strain response can now be obtained from microtensile and microcompression specimens. Inverse methods for measuring mechanical properties are appealing, but the accuracy of these measurements is highly dependent on boundary conditions and geometry, and associated uncertainties currently limit the applicability of such techniques. Elevated temperature microtensile experiments are being conducted, but such tests are especially challenging, relatively rare, and represent an opportunity for future research.

Annu. Rev. Mater. Res. 2007.37:93-126. Downloaded from arjournals.annualreviews.org
by University of Virginia Libraries on 02/20/08. For personal use only.

Results from microspecimen tests have provided valuable insight into size-scale effects on the elastic, brittle, and ductile behavior at the microscale. Fundamental elastic interactions, which depend on atomic-level bonding, do not show a size effect in MEMS specimens; the moduli measured in microtensile experiments are consistent with commonly accepted bulk values and can be predicted from anisotropic elastic constants when crystallographic texture is properly taken into account. Reduced modulus values have been measured in vapor-deposited nanocrystalline metallic thin films; anomalous grain boundary compliance has been suggested, but the influence of grain boundary cracks and voids cannot be discounted. Intrinsic fracture toughness is also size independent, but the fracture strength of brittle MEMS materials, as measured in microtensile experiments, has proven to be extremely dependent on the size and distribution of flaws, especially surface roughness.

Clear and indisputable measurements point to the presence of both intrinsic and extrinsic size effects on the strength of ductile materials. These findings imply that the operation of intrinsic dislocation processes in greatly reduced or confined volumes significantly alters the ways in which dislocations are generated, multiply, and interact. Models are needed to explain the storage of geometrically necessary dislocations during strain gradient plasticity, the change and evolution of dislocation behavior in nanocrystalline metals, and the stochastic nature of dislocation motion in micron-sized specimens. Preliminary models have been put forth, but higher fidelity experiments and models are needed, and this will remain an exciting area of research for the foreseeable future.

FUTURE ISSUES

1. The advances in both test methods and in the understanding of material behavior at the microscale have been remarkable over the past 10–15 years, and one can expect similar, if not accelerated, progress in the future. New experimental methods and advanced models will address a broad range of mechanical properties (e.g., fracture toughness, fatigue life, and creep) and service conditions (e.g., temperature extremes and corrosive environments).
2. Many small-scale components and devices operate at temperatures other than room temperature. Ranges are from −40°C to 200°C for automotive and space applications and up to 1200°C for protective coatings. Test methods that enable tensile testing in these ranges and that should be readily extendable to measure time-dependent creep properties are beginning to emerge. Testing at both low and high temperatures has its own special set of challenges, and progress in test methods is needed.
3. Fatigue life is especially important for certain kinds of MEMS such as radio frequency (RF) switches and digital mirrors. Research on microscale metal and ceramic structures is still in its infancy. Questions about how changes in dislocation activity affect crack nucleation in metallic microdevices and whether surface roughness accelerates fatigue in ceramic microstructures

remain to be addressed. MEMS devices may see billions of cycles, and high-cycle fatigue is especially important. In that regard, the recent introduction of integrated test methods that operate at 20 KHz (one billion cycles in 14 h) is noteworthy and exciting. The general area of both low-cycle and high-cycle fatigue at these size scales is rich indeed.

4. Developments in mechanical testing of MEMS materials have spawned new approaches to study the behavior of other materials at the nanoscale—witness the integral specimen/test machine approach. One can expect that other new microdevices will arise and enable the preparation, handling, and testing of specimens with features down to nanometers. Challenges include not only the fabrication and actuation of such devices but also imaging and the determination of stress and strain in such small structures.
5. The ability to measure the strength of ductile single-phase metals with micron-sized specimens and nanocrystalline specimens has unveiled obvious size effects with respect to their flow strength. The emerging view is that dislocation plasticity is fundamentally different in reduced volumes of materials. The need for new plasticity models that take account of the discrete nature of dislocation slip in finite volumes of material is unmistakable, and this appears to be a very exciting area for future research.

Annu. Rev. Mater. Res. 2007.37:93-126. Downloaded from arjournals.annualreviews.org
by University of Virginia Libraries on 02/20/08. For personal use only.

ACKNOWLEDGMENTS

Research in these areas has been supported by separate and joint grants from various federal agencies including NSF, DARPA, AFOSR, the Army Research Laboratory, the Naval Surface Warfare Center, and NASA. The Johns Hopkins University, the Whiting School of Engineering, and the Department of Mechanical Engineering have provided not only facilities but a stimulating environment as well. An exceptional group of undergraduate researchers, graduate students, and postdoctoral fellows has developed new test methods and obtained exciting results. Both authors are grateful for the challenges and opportunities these have presented.

LITERATURE CITED

1. Sharpe Jr WN. 2001. Mechanical properties of MEMS materials. In *The MEMS Handbook*, ed. M Gad-el-Hak, pp. 3:1–33. Boca Raton, FL: CRC Press
2. Spearing SM. 2000. Materials issues in microelectromechanical systems (MEMS). *Acta Mater*. 48:179–96
3. Yi T, Chang-Jin K. 1999. Measurement of mechanical properties for MEMS materials. *Meas. Sci. Technol*. 10(8):706–16
4. Haque MA, Saif MTA. 2003. A review of MEMS-based microscale and nanoscale tensile and bending testing. *Experimental Mech*. 43(3):248–55

5. ASTM Int. 2004. *ASTM E8M-04, Standard Test Methods for Tension Testing of Metallic Materials*. West Conshohocken, PA: ASTM Int.
6. Doerner MF, Nix WD. 1986. A method for interpreting the data from depth sensing indentation instruments. *J. Mater. Res.* 1:601–9
7. Oliver WC, Pharr GM. 1992. An improved technique for determining hardness and elastic modulus using load and displacement sensing indentation experiments. *J. Mater. Res.* 7:1564–74
8. McElhaney KW, Vlassak JJ, Nix WD. 1998. Determination of indenter tip geometry and indentation contact area for depth-sensing indentation experiments. *J. Mater. Res.* 13:1300–6
9. Pharr GM. 1998. Measurement of mechanical properties by ultralow load indentation. *Mater. Sci. Eng. A* 253:151–59
10. Nix WD. 1997. Elastic and plastic properties of thin films on substrates: nanoindentation techniques. *Mater. Sci. Eng. A* 234–236:37–44
11. Suresh S, Giannakopoulos AE. 1998. A new method for estimating residual stresses by instrumented sharp indentation. *Acta Mater.* 46:5755–67
12. Saha R, Nix WD. 2002. Effects of the substrate on the determination of thin film mechanical properties by nanoindentation. *Acta Mater.* 50:23–38
13. Nix WD, Gao H. 1998. Indentation size effects in crystalline materials: a law for strain gradient plasticity. *J. Mech. Phys. Solids* 46:411–25
14. Gao H, Huang Y, Nix WD, Hutchinson JW. 1999. Mechanism-based strain gradient plasticity. I. Theory. *J. Mech. Phys. Solids* 47:1239–63
15. Huang Y, Gao H, Nix WD, Hutchinson JW. 2000. Mechanism-based strain gradient plasticity. II. Analysis. *J. Mech. Phys. Solids* 48:99–128
16. Thouless MD. 1995. Modeling the development and relaxation of stresses in films. *Annu. Rev. Mater. Sci.* 25:69–96
17. Freund LB, Suresh S. 2003. *Thin Film Materials: Stress, Defect Formation and Surface Evolution*. Cambridge, UK: Cambridge Univ. Press
18. Macionczyk M, Bruckner W. 1999. Tensile testing of AlCu thin films on polyimide foils. *J. Appl. Phys.* 86:4922–29
19. Hommel M, Kraft O. 2001. Deformation behavior of thin copper films on deformable substrates. *Acta Mater.* 49:3935–47
20. Xiang Y, Li T, Suo Z, Vlassak JJ. 2005. High ductility of a metal film adherent on a polymer substrate. *Appl. Phys. Lett.* 87:1–3
21. Begley MR, Bart-Smith H. 2005. The electro-mechanical response of highly compliant substrates and thin stiff films with periodic cracks. *Int. J. Solids Struct.* 42:5259–73
22. Vlassak JJ, Nix WD. 1992. New bulge test technique for the determination of Young's modulus and Poisson's ratio of thin films. *J. Mater. Res.* 7:3242–49
23. Xiang Y, Vlassak JJ. 2005. Bauschinger effect in thin metal films. *Scr. Mater.* 53:177–82
24. Xiang Y, Chen X, Vlassak JJ. 2005. Plane-strain bulge test for thin films. *J. Mater. Res.* 20:2360–70
25. Nicola L, Xiang Y, Vlassak JJ, Van der Giessen E, Needleman A. 2006. Plastic deformation of freestanding thin films: experiments and modeling. *J. Mech. Phys. Solids* 54:2089–110

Annu. Rev. Mater. Res. 2007.37:93-126. Downloaded from arjournals.annualreviews.org
by University of Virginia Libraries on 02/20/08. For personal use only.

26. Jayaraman S, Edwards RL, Hemker KJ. 1999. Relating mechanical testing and microstructural features of polysilicon thin films. *J. Mater. Res.* 14(2):688–97
27. Edwards RL, Coles G, Sharpe Jr WN. 2004. Comparison of tensile and bulge tests for thin film silicon nitride. *Exp. Mech.* 44:49–54
28. Weihs TP, Hong S, Bravman JC, Nix WD. 1988. Mechanical deflection of cantilever microbeams: a new technique for testing the mechanical properties of thin films. *J. Mater. Res.* 3:931–42
29. Florando JN, Nix WD. 2005. A microbeam bending method for studying stress-strain relations for metal thin films on silicon substrates. *J. Mech. Phys. Solids* 53:619–38
30. Motz C, Schoberl T, Pippan R. 2005. Mechanical properties of microsized copper bending beams machined by the focused ion beam technique. *Acta Mater.* 53:4269–79
31. Kobrinsky MJ, Deutsch ER, Senturia SD. 2000. Effect of support compliance and residual stress on the shape of doubly supported surface-micromachined beams. *J. Microelectromech. Sys.* 9(3):361–69
32. Sharpe Jr WN, Yuan B, Vaidyanathan R, Edwards RL. 1996. New test structures and techniques for measurement of mechanical properties of MEMS materials. *Proc. SPIE Symp. Microlithogr. Metrol. Micromach. II, Austin*, pp. 78–91. Bellingham, WA: Int. Soc. Opt. Eng.
33. Gianola DS, Van Petegem S, Legros M, Brandstetter S, Van Swygenhoven H, Hemker KJ. 2006. Stress assisted discontinuous grain growth and its effect on the deformation behavior of nanocrystalline aluminum thin films. *Acta Mater.* 54:2253–63
34. Sharpe Jr WN, Turner KT, Edwards RL. 1999. Tensile testing of polysilicon. *Exp. Mech.* 39:162–70
35. Hemker KJ, Last H. 2001. Microsample tensile testing of LIGA nickel for MEMS applications. *Mater. Sci. Eng. A* 319–321:882–86
36. Becker EW, Ehrfeld W, Hagmann P, Maner A, Muenchmeyer D. 1986. Fabrication of microstructures with high aspect ratios and great structural heights by synchrotron radiation lithography, galvanoforming and plastic moulding (LIGA process). *Microelectron. Eng.* 4:35–56
37. Klaassen EH, Petersen K, Noworolski JM, Logan J, Maluf NI, et al. 1996. Silicon fusion bonding and deep reactive ion etching: a new technology for microstructures. *Sens. Actuators A* 52:132–39
38. Sharpe Jr WN, Beheim G, Nemeth N, Evans L, Jadaan O. 2005. Strength of single-crystal silicon carbide microspecimens at room and high temperature. *Proc. 2005 SEM Annual Conf., Portland, OR*, Session 46, Paper 54 on CD. Bethel, CT: Soc. Exp. Mech.
39. LaVan DA, Sharpe WN Jr. 2001. Local properties of undermatched steel weld metal. *Metallurg. Mater. Trans. A* 32:913–22
40. Pan D, Chen MW, Wright PK, Hemker KJ. 2003. Characterization of a diffusion aluminide bond coat for thermal barrier coatings. *Acta Mater.* 51:2205–17
41. Boehlert CJ, Zupan M, Dimiduk DM, Hemker KJ. 1999. Microsample creep testing of fully-lamellar TiAl alloys. In *Gamma Titanium Aluminides*, ed. Y-W Kim, DM Dimiduk, MH Loretto, pp. 669–77. Warrendale, PA: TMS Publ.

Annu. Rev. Mater. Res. 2007.37:93-126. Downloaded from arjournals.annualreviews.org
by University of Virginia Libraries on 02/20/08. For personal use only.

42. Zupan M, Hemker KJ. 2001. High temperature microsample tensile testing of γ-TiAl. *Mater. Sci. Eng. A* 319–321:810–14
43. Zupan M, Hemker KJ. 2003. Yielding behavior of aluminum-rich single crystalline γ-TiAl. *Acta Mater*. 51(20):6277–90
44. Legros M, Elliott BR, Rittner MN, Weertman JR, Hemker KJ. 2000. Microsample tensile testing of nanocrystalline metals. *Philos. Mag. A* 80:1017–26
45. Wang YM, Wang K, Pan D, Lu K, Hemker KJ, Ma E. 2003. Microsample tensile testing of nanocrystalline copper. *Scr. Mater*. 48:1581–86
46. Coe D. 1999. *The application of microsample testing to an investigation of electron irradiation effects on type 316 stainless steel and Fe-Cu-Mn*. M.S. dissertation. Johns Hopkins Univ.
47. Uchic MD, Dimiduk DM, Florando JN, Nix WD. 2004. Sample dimensions influence strength and crystal plasticity. *Science* 305(5686):986–89
48. Thompson RJ, Hemker KJ, Uchic MD. 2004. Experimental techniques for scale-specific tension testing of aerospace alloys. *TMS Lett*. 1:143–44
49. Eby MA, Sharpe Jr WN, Coles G. 2001. Mechanical properties of polysilicon between 0°C and 250°C. *Proc. MEMS: Mech. Meas. Symp., Portland, OR*, pp. 16–19. Soc. Exp. Mech.
50. Sharpe Jr WN, Pulskamp J, Gianola D, Eberl C, Polcawich R, Thompson R. 2007. Strain measurements of silicon dioxide microspecimens by digital imaging processing. *Exp. Mech*. In press
51. Zhang H, Schuster BE, Wei Q, Ramesh KT. 2006. The design of accurate microcompression experiments. *Scr. Mater*. 54:181–86
52. Greek S, Johansson S. 1997. Tensile testing of thin film microstructures. *Proc. SPIE* 3224:344–51
53. Espinosa HD, Prorok BC, Fischer M. 2003. A novel method for measuring elasticity, plasticity and fracture of thin films and MEMS materials. *J. Mech. Phys. Solids* 51:47–67
54. Espinosa HD, Prorok BC, Peng B. 2004. Plasticity size effects in free-standing submicron polycrystalline FCC films subjected to pure tension. *J. Mech. Phys. Solids* 52:667–89
55. Haque MA, Saif MTA. 2002. In-situ tensile testing of nano-scale specimens in SEM and TEM. *Exp. Mech*. 42:123–28
56. Haque MA, Saif MTA. 2002. Mechanical behavior of 30–50 nm thick aluminum films under uniaxial tension. *Scr. Mater*. 47:863–67
57. Sharpe Jr WN. 1989. An interferometric strain/displacement measurement system. *NASA Tech. Memo.* 101638
58. Sharpe Jr WN, Yuan B, Edwards RL. 1997. A new technique for measuring the mechanical properties of thin films. *J. Microelectromech. Sys*. 6(3):193–98
59. Cho HS, Hemker KJ, Lian K, Goettert J, Dirras G. 2003. Measured mechanical properties of LIGA Ni structures. *Sens. Actuators A* 103:59–63
60. Read DT, Dally JW. 1992. A new method for measuring the constitutive properties of thin films. *J. Mater. Res*. 8:1542–49
61. Emery RD, Povirk GL. 2003. Tensile behavior of free-standing gold films. I. Coarse-grained films. *Acta Mater*. 51(7):2067–78

Annu. Rev. Mater. Res. 2007.37:93-126. Downloaded from arjournals.annualreviews.org
by University of Virginia Libraries on 02/20/08. For personal use only.

Annu. Rev. Mater. Res. 2007.37:93-126. Downloaded from arjournals.annualreviews.org
by University of Virginia Libraries on 02/20/08. For personal use only.

62. Tong W. 2005. An evaluation of digital image correlation criteria for strain mapping applications. *Strain* 41(4):167–75
63. Biery N, De Graef M, Pollock TM. 2003. A method for measuring microstructural-scale strains using a scanning electron microscope: applications to γ-titanium aluminides. *Metallurg. Mater. Trans. A* 34:2301–13
64. Chasiotis I, Knauss WG. 2000. Microtensile tests with the aid of probe microscopy for the study of MEMS materials. *Proc. SPIE* 4175:96–103
65. Zupan M, Hayden MJ, Boehlert CJ, Hemker KJ. 2001. Development of high temperature microsample testing. *Exp. Mech*. 41:242–47
66. Cho HS, Hemker KJ, Lian K, Goettert J. 2002. Tensile, creep and fatigue properties of LIGA nickel structures. *Proc. IEEE Electromech. Sys. (MEMS), 15th, Las Vegas*, pp. 439–42
67. Jain P. 2006. *Microscale characterization of coatings for a high strength high conductivity alloy*. PhD thesis. Johns Hopkins Univ.
68. Savage MF, Tatalovich J, Zupan M, Hemker KJ, Mills MJ. 2001. Deformation mechanisms and microtensile behavior of single colony Ti-6242Si. *Mater. Sci. Eng. A* 319–321:398–403
69. Sharpe Jr WN. 2003. Murray lecture tensile testing at the micrometer scale: opportunities in experimental mechanics. *Exp. Mech*. 43(3):228–37
70. Sharpe Jr WN, Eby MA, Coles G. 2001. Effect of temperature on mechanical properties of polysilicon. *Proc. Transducers '01* 1366–69
71. Sharpe Jr WN, Jackson KM, Hemker KJ, Xie Z. 2001. Effect of specimen size on Young's modulus and fracture strength of polysilicon. *J. Microelectromech. Sys*. 10:317–26
72. Sharpe Jr WN, Yuan B, Edwards RL, Vaidyanathan R. 1997. Measurements of Young's modulus, Poisson's ratio, and tensile strength of polysilicon. *Proc. IEEE Electromech. Sys. (MEMS), 10th, Nagoya, Japan*, pp. 424–29
73. Jackson KM. 2005. Fractures strength, elastic modulus and Poisson's ration of polycrystalline 3C thin film found by microsample tensile testing. *Sens. Actuators A* 1(125):34–40
74. Deleted in proof
75. Jackson KM, Dunning J, Zorman CA, Mehregany M, Sharpe Jr WN. 2005. Mechanical properties of epitaxial 3C silicon carbide thin films. *J. Microelectromech. Sys*. 14(4):664–72
76. Fritz T, Cho HS, Hemker KJ, Mokwa W, Schnakenberg U. 2002. Characterization of electroplated nickel. *Microsys. Technol*. 9:87–91
77. He Y, Schwarz RB, Darling T, Hundely M, Whang SH, Wang SC. 1997. Elastic constants and thermal expansion of single crystal γ-TiA1 from 300 to 750 K. *Mater. Sci. Eng. A* 239–240:157–63
78. Huang H, Spaepen F. 2000. Tensile testing of free-standing Cu, Ag and Al thin films and Ag/Cu multilayers. *Acta Mater*. 48:3261–69
79. Sharpe Jr WN, Pulskamp J, Mendis BG, Eberl C, Gianola DS, et al. 2006. Tensile stress-strain curves of gold film. *Proc. ASME Int. Mech. Eng. Congr. Expo., Chicago*, 13290

Annu. Rev. Mater. Res. 2007.37:93-126. Downloaded from arjournals.annualreviews.org
by University of Virginia Libraries on 02/20/08. For personal use only.

80. Haque MA, Saif MTA. 2004. Deformation mechanisms in free-standing nanoscale thin films: a quantitative in situ transmission electron microscope study. *Proc. Natl. Acad. Sci. USA* 101:6335–40
81. Chen MW, Ma E, Hemker KJ, Sheng H, Yinmin Wang Y, Cheng XM. 2003. Deformation twinning in nanocrystalline aluminum. *Science* 300:1275–77
82. Gianola DS, Mendis BG, Cheng XM, Hemker KJ. 2007. Grain size stabilization by impurities and effect on stress-coupled grain growth in nanocrystalline Al thin films. *Mater. Sci. Eng. A*. In press
83. Deleted in proof
84. Bagdahn J, Sharpe Jr WN, Jadaan O. 2003. Fracture strength of polysilicon at stress concentrations. *J. Microelectromech. Sys*. 12:302–12
85. Sharpe Jr WN, Jackson K, Coles G. 2001. Young's modulus and fracture strength of three polysilicons. *Mater. Sci. Microelectromech. Sys. (MEMS) Devices III*, *MRS Proc.* 657:EE 5.5.1–6
86. Chasiotis I, Knauss WG. 2004. The mechanical strength of polysilicon films. II. Size effects associated with elliptical and circular perforations. *J. Mech. Phys. Solids* 51:1551–72
87. Ballarini R, Kahn H, Tayebi N, Heuer AH. 2001. Effects of microstructure on the strength and fracture toughness of polysilicon: a wafer level testing approach. *ASTM Spec. Tech. Publ*. 1413:37–51
88. Kahn H, Tayebi N, Ballarini R, Mullen RL, Heuer AH. 1999. Fracture toughness of polysilicon MEMS devices. *Sens. Actuators* 82:274–80
89. Namazu T, Isono Y, Tanaka T. 2000. Evaluation of size effect on mechanical properties of single crystal silicon by nanoscale bending tests using AFM. *J. Microelectromech. Sys*. 9:450–59
90. Sharpe Jr WN, Jadaan O, Beheim GM, Quinn GD, Nemeth NN. 2005. Fracture strength of silicon carbide microspecimens. *J. Microelectromech. Sys*. 14:903–13
91. Deleted in proof
92. Chen MW, Ma E, Hemker KJ. 2006. Mechanical behavior of nanocrystalline materials. In *CRC Nanomaterials Handbook*, ed. Y Gogotsi, pp. 497–531. Boca Raton, FL: CRC Press
93. Van Swygenhoven H, Derlet PM, Hasnaoui A. 2002. Cooperative processes during plastic deformation in nanocrystalline fcc metals: a molecular dynamics simulation. *Phys. Rev. B* 66(18):1841121–28
94. Yamakov V, Wolf D, Phillpot SE, Mukherjee AK, Gleiter H. 2002. Dislocation processes in the deformation of nanocrystalline aluminum by molecular-dynamics simulation. *Nat. Mater*. 1(1):45–48
95. Schiøtz J, Jacobsen KW. 2003. A maximum in the strength of nanocrystalline copper. *Science* 301(5638):1357–59
96. Van Swygenhoven H, Derlet PM, Froseth AG. 2004. Stacking fault energies and slip in nanocrystalline metals. *Nat. Mater*. 3(6):399–403
97. Kumar KS, Suresh S, Chisholm MF, Horton JA, Wang P. 2003. Deformation of electrodeposited nanocrystalline nickel. *Acta Mater*. 51(2):387–405

98. Budrovic Z, Van Swygenhoven H, Derlet PM, Van Petegem S, Schmitt B. 2004. Plastic deformation with reversible peak broadening in nanocrystalline metal. *Science* 304(5668):273–76
99. Jin M, Minor AM, Stach EA, Morris Jr JW. 2004. Direct observation of deformation-induced grain growth during the nanoindentation of ultrafine-grained Al at room temperature. *Acta Mater*. 52(18):5381–87
100. Zhang K, Weertman JR, Eastman JA. 2004. The influence of time, temperature, and grain size on indentation creep in high-purity nanocrystalline and ultrafine grain copper. *Appl. Phys. Lett*. 85:5197–99
101. Zhang K, Weertman JR, Eastman JA. 2005. Rapid stress-driven grain coarsening Cu at ambient and cryogenic temperatures. *Appl. Phys. Lett*. 87:1–3
102. Winning M, Gottstein G, Shvindlerman LS. 2001. Stress induced grain boundary motion. *Acta Mater*. 49(2):211–19
103. Winning M, Gottstein G, Shvindlerman LS. 2002. On the mechanisms of grain boundary migration. *Acta Mater*. 50(2):353–63
104. Cahn JW, Taylor JE. 2004. A unified approach to motion of grain boundaries, relative tangential translation along grain boundaries, and grain rotation. *Acta Mater*. 52:4887–98
105. Cahn JW, Mishin Y, Suzuki A. 2006. Duality of dislocation content of grain boundaries. *Philos. Mag.* 86(25–26):3965–80
106. Cahn JW, Mishin Y, Suzuki A. 2006. Coupling grain boundary motion to shear deformation. *Acta Mater*. 54(19):4953–75
107. Arzt E. 1998. Size effects in materials due to microstructural and dimensional constraints: a comparative review. *Acta Mater*. 46:5611–26
108. Fleck NA, Muller GM, Ashby MF, Hutchinson JW. 1994. Strain gradient plasticity theory and experiment. *Acta Metall. Mater*. 42:475–87
109. Stolken JS, Evans AG. 1998. A microbend test method for measuring the plasticity length scale. *Acta Mater*. 46:5109–15
110. Ma Q, Clarke DR. 1995. Size dependent hardness of silver single crystals. *J. Mater. Res*. 10:853–63
111. Greer JR, Oliver WC, Nix WD. 2005. Size dependence of mechanical properties of gold at the micron scale in the absence of strain gradients. *Acta Mater*. 53:1821–30
112. Volkert CA, Lilleodden ET. 2006. Size effects in the deformation of submicron Au columns. *Philos. Mag*. 86:5567–79
113. Dimiduk DM, Uchic MD, Parthasarathy TA. 2005. Size-affected single-slip behavior of pure nickel microcrystals. *Acta Mater*. 53:4065–77
114. Venkatraman R, Bravman JC. 1992. Separation of film thickness and grain boundary strengthening effects in Al thin films. *J. Mater. Res*. 8:2040–48
115. Nix WD. 1989. Mechanical properties of thin films. *Metall. Trans. A* 20:2217–45
116. Xiang Y, Tsui TY, Vlassak JJ. 2006. The mechanical properties of freestanding electroplated Cu thin films. *J. Mater. Res*. 21(6):1607–18
117. LaVan DA, Tsuchiya T, Coles G, Knauss WG, Chasiotis I, Read D. 2001. Cross comparison of direct tensile testing techniques on polysilicon films. In *Mechanical Properties of Structural Films* (STP1413), eds. CL Muhlstein, SB Brown, pp. 16–27. West Conshohocken, PA: Am. Soc. Test. Mater.

Annu. Rev. Mater. Res. 2007.37:93-126. Downloaded from arjournals.annualreviews.org
by University of Virginia Libraries on 02/20/08. For personal use only.

118. Tsuchiya T, Tabata O, Sakata J, Taga Y. 1998. Specimen size effect on tensile strength of surface-micromachined polycrystalline silicon thin films. *J. Micromech. Sys.* 7:106–13
119. Greek S, Ericson F, Johansson S, Schweitz J-Å. 1997. In situ tensile strength measurement and Weibull analysis of thick film and thin film micromachined polysilicon structures. *Thin Solid Films* 29:247–54
120. Ding JN, Meng YG, Wen SZ. 2001. Size effect on the mechanical properties of microfabricated polysilicon thin films. *J. Mater. Res.* 16:2223–28

Annu. Rev. Mater. Res. 2007.37:93-126. Downloaded from arjournals.annualreviews.org
by University of Virginia Libraries on 02/20/08. For personal use only.

Annual Review of Materials Research

Volume 37, 2007

Contents

Annu. Rev. Mater. Res. 2007.37:93-126. Downloaded from arjournals.annualreviews.org
by University of Virginia Libraries on 02/20/08. For personal use only.

MATERIALS CHARACTERIZATION

Low-Temperature Degradation of Zirconia and Implications for Biomedical Implants
Jérôme Chevalier, Laurent Gremillard, and Sylvain Deville 1

Single-Molecule Micromanipulation Techniques
K. C. Neuman, T. Lionnet, and J.-F. Allemand 33

Spin-Polarized Scanning Tunneling Microscopy of Magnetic Structures and Antiferromagnetic Thin Films
Wulf Wulfhekel and Jürgen Kirschner 69

Microscale Characterization of Mechanical Properties
K. J. Hemker and W. N. Sharpe, Jr. 93

Three-Dimensional Atom-Probe Tomography: Advances and Applications
David N. Seidman 127

The Study of Nanovolumes of Amorphous Materials Using Electron Scattering
David J. H. Cockayne 159

Nanoscale Electromechanics of Ferroelectric and Biological Systems: A New Dimension in Scanning Probe Microscopy
Sergei V. Kalinin, Brian J. Rodriguez, Stephen Jesse, Edgar Karapetian, Boris Mirman, Eugene A. Eliseev, and Anna N. Morozovska 189

AFM and Acoustics: Fast, Quantitative Nanomechanical Mapping
Bryan D. Huey 351

Electron Holography: Applications to Materials Questions
Hannes Lichte, Petr Formanek, Andreas Lenk, Martin Linck, Christopher Matzeck, Michael Lehmann, and Paul Simon 539

Three-Dimensional Characterization of Microstructure by Electron Back-Scatter Diffraction
Anthony D. Rollett, S.-B. Lee, R. Campman, and G.S. Rohrer 627

Atom Probe Tomography of Electronic Materials
Thomas F. Kelly, David J. Larson, Keith Thompson, Roger L. Alvis, Joseph H. Bunton, Jesse D. Olson, and Brian P. Gorman 681

Electron Holography: Phase Imaging with Nanometer Resolution
Martha R. McCartney and David J. Smith 729

FERROELECTRICS AND RELATED MATERIALS, *David R. Clarke and Venkatraman Gopalan, Guest Editors*

Atomic-Level Simulation of Ferroelectricity in Oxides: Current Status and Opportunities
Simon R. Phillpot, Susan B. Sinnott, and Aravind Asthagiri 239

Ferroelectric Domain Breakdown
Michel Molotskii, Yossi Rosenwaks, and Gil Rosenman 271

Local Structure of Ferroelectric Materials
T. Egami 297

Terahertz Polaritonics
T. Feurer, Nikolay S. Stoyanov, David W. Ward, Joshua C. Vaughan, Eric R. Statz, and Keith A. Nelson 317

Spiral Magnets as Magnetoelectrics
T. Kimura 387

Universal Domain Wall Dynamics in Disordered Ferroic Materials
W. Kleemann 415

Defect–Domain Wall Interactions in Trigonal Ferroelectrics
Venkatraman Gopalan, Volkmar Dierolf, and David A. Scrymgeour 449

Influence of Electric Field and Mechanical Stresses on the Fracture of Ferroelectrics
Gerold A. Schneider 491

Strain Tuning of Ferroelectric Thin Films
Darrell G. Schlom, Long-Qing Chen, Chang-Beom Eom, Karin M. Rabe, Stephen K. Streiffer, and Jean-Marc Triscone 589

Ferroelectric Epitaxial Thin Films for Integrated Optics
Bruce W. Wessels 659

Index

Cumulative Index of Contributing Authors, Volumes 33–37 769

Errata

An online log of corrections to *Annual Review of Materials Research* chapters (if any, 1997 to the present) may be found at http://matsci.annualreviews.org/errata.shtml

Annu. Rev. Mater. Res. 2007.37:93-126. Downloaded from arjournals.annualreviews.org
by University of Virginia Libraries on 02/20/08. For personal use only.